

Learning Invariant Causal Mechanism from Vision-Language Models

Zeen Song*

Institute of Software
Chinese Academy of Sciences
University of China Academy of Sciences
Beijing China
songzeen@iscas.ac.cn

Siyu Zhao*

University of China Academy of Sciences
Beijing China
zhaosiyu23@mails.ucas.ac.cn

Xingyu Zhang*

Institute of Software
Chinese Academy of Sciences
University of China Academy of Sciences
Beijing China
zhangxingyu@iscas.ac.cn

Jiangmeng Li

Institute of Software
Chinese Academy of Sciences
University of China Academy of Sciences
Beijing China
lijiangmeng@iscas.ac.cn

Changwen Zheng

Institute of Software
Chinese Academy of Sciences
University of China Academy of Sciences
Beijing China
zhengchangwen@iscas.ac.cn

Wenwen Qiang†

Institute of Software
Chinese Academy of Sciences
University of China Academy of Sciences
Beijing China
qiangwenwen@iscas.ac.cn

Abstract

Large-scale pre-trained vision-language models such as CLIP have been widely applied to a variety of downstream scenarios. In real-world applications, the CLIP model is often utilized in more diverse scenarios than those encountered during its training, a challenge known as the out-of-distribution (OOD) problem. However, our experiments reveal that CLIP performs unsatisfactorily in certain domains. Through a causal analysis, we find that CLIP’s current prediction process cannot guarantee a low OOD risk. The lowest OOD risk can be achieved when the prediction process is based on invariant causal mechanisms, i.e., predicting solely based on invariant latent factors. However, theoretical analysis indicates that CLIP does not identify these invariant latent factors. Therefore, we propose the Invariant Causal Mechanism for CLIP (CLIP-ICM), a framework that first identifies invariant latent factors using interventional data and then performs invariant predictions across various domains. Our method is simple yet effective, without significant computational overhead. Experimental results demonstrate that CLIP-ICM significantly improves CLIP’s performance in OOD scenarios.

*Equal contribution

†Corresponding author

1 Introduction

As one of the most successful large-scale pre-trained vision-language models, Contrastive Language-Image Pretraining (CLIP) Radford et al. [2021] has garnered significant attention. It has been widely applied in various downstream tasks Gao et al. [2023], Zhou et al. [2022a,b], Shu et al. [2023]. Particularly noteworthy is CLIP’s capability for zero-shot prediction. Given a test image and a set of category labels with natural language descriptions, CLIP can classify the image into the closest category based on the similarity between the image and the natural language descriptions of the labels.

However, in real-world applications, the CLIP model is expected to be adaptable to diverse scenarios with data distributions different from those encountered during training Torralba and Efros [2011], Fang et al. [2013], Beery et al. [2018], Gulrajani and Lopez-Paz [2020], Abbe et al. [2023]. These scenarios are commonly referred to as out-of-distribution (OOD) problems. Given the challenges posed by OOD scenarios, we assess CLIP’s classification performance across different domains within the VLCS Fang et al. [2013] dataset. However, experimental results reveal inconsistent performance of CLIP when applied to various domains. In particular, CLIP shows poor performance when faced with the OOD problem in zero-shot scenarios.

We explore the underlying reasons for this phenomenon through a causal lens, as humans often conceptualize the aspects of the physical world in terms of causal relationships Schölkopf et al. [2021]. We first establish a Structural Causal Model (SCM) to model the prediction problem of CLIP when facing different environments. In the SCM, we hypothesize that the data are generated by two types of latent factors: the invariant factors, which are not influenced by the environment, and the variant factors, which are determined by the environment, and an accurate prediction is performed when using both the invariant and variant factors. Through analysis, we prove that a classifier trained on the known environments can correctly perform prediction in an unknown environment only when the distribution of variant latent factors in this environment is known. Please refer to Section 3.3 for more detail.

We further analyze the OOD error risk associated with current CLIP prediction approaches, specifically zero-shot and linear-probe predictions. We demonstrate that without knowledge of the variant factors in the target environment, the OOD error risk is influenced by the $\mathcal{H}\Delta\mathcal{H}$ -divergence between the unseen and training environments Ben-David et al. [2010]. Moreover, we prove that if a classifier is learned using only the invariant factors, the error risks remain consistent across all environments. Consequently, if an invariant predictor achieves lower empirical risk, it will exhibit lower OOD risk compared to a regular predictor. Therefore, to mitigate the poor OOD performance associated with CLIP, our objective is to find a well-performing invariant predictor that classifies based solely on the invariant factors.

A key challenge, as our theoretical analysis reveals, is that the representation learning process of CLIP does not ensure the learning of invariant factors. To address this, we propose CLIP-ICM, a framework designed to enable the CLIP model to identify invariant latent factors. This framework also allows CLIP to perform zero-shot prediction and linear evaluation using only these factors. Unlike existing methods, CLIP-ICM does not require training with labeled data and can be applied to downstream tasks in unseen environments in a zero-shot manner. Experimental results on commonly used OOD datasets demonstrate the outstanding effectiveness of our approach, achieving superior performance under zero-shot and linear-probe conditions.

Our contributions can be summarized as follows: **(i)** We discover that CLIP suffers from poor performance in OOD scenarios. Through an in-depth causal analysis, we provide a formulation of the causal mechanism of prediction across different domains. **(ii)** Based on this formulation, we prove that the OOD risk in CLIP’s current prediction process is influenced by the divergence between unseen and training environments. We further demonstrate that lower OOD risk can be achieved when prediction is performed using the invariant causal mechanism, i.e., learning with only the invariant latent factors, provided it performs well during training. **(iii)** Learning invariant causal mechanisms presents a major challenge, as it requires identifying the invariant latent factors. Our theoretical analysis shows that invariant latent factors can be identified under specific conditions. Based on these findings, we propose CLIP-ICM, a framework that enables CLIP to identify invariant latent factors and perform invariant predictions in both zero-shot and linear-probe manners. **(iv)** Experimental results confirm that CLIP-ICM is highly effective compared to state-of-the-art methods, significantly

improving CLIP’s performance in OOD scenarios. We also conduct a series of ablation studies to validate the effectiveness of our proposed CLIP-ICM.

2 Related Work

Vision-Language Pre-training. Incorporating language with the visual modality has been a long-standing issue, as extensively researched in previous works Frome et al. [2013], Socher et al. [2013], Norouzi et al. [2014], Elhoseiny et al. [2013]. Recent years have seen significant success in multi-modal pre-training models, spearheaded by CLIP Radford et al. [2021] and ALIGN Jia et al. [2021], with the aim of enabling cross-modal learning by mapping language and visual modalities into the same embedding space. Notably, researchers have turned their focus towards improving CLIP’s OOD performance in downstream tasks Gao et al. [2023], Zhou et al. [2022a,b], Shu et al. [2023]. In our work, we delve into the reasons behind CLIP’s poor OOD generalization ability from a causal perspective. We propose CLIP-ICM as a solution to address this issue.

Causal Representation Learning. The latent factor hypothesis assumes that a set of latent factors generate the observational data Bishop [1998]. A core task in causal representation learning is to provably identify these latent factors Bengio et al. [2014], Schölkopf et al. [2021], Schoelkopf et al. [2012]. Additionally, the issue of identification is commonly referred to as the Independent Component Analysis (ICA) problem Hyvärinen and Oja [2000], which aims to separate independent signals from those mixed during observation. While the problem of ICA has been proven to be achievable in the linear case Hyvärinen and Oja [2000], non-linear ICA has been shown to be impossible without inductive biases relying on auxiliary labels Hyvärinen and Pajunen [1999], Locatello et al. [2019], Hyvarinen and Morioka [2017], Locatello et al. [2020], imposing sparsity Schölkopf et al. [2021], Lachapelle et al. [2022], or restricting the function class Zimmermann et al. [2022]. While the studies mentioned above concentrate on scenarios with only observational data Roeder et al. [2021], Kügelgen et al. [2021], Zimmermann et al. [2022], an increasing number of studies are now focusing on cases where interventional data is available Ahuja et al. [2023], Buchholz et al. [2023], Squires et al. [2023]. We approach from a similar perspective and propose a simple and effective way to utilize intervention data to identify the invariant features of CLIP.

Out-of-distribution Generalization. It is evident in many cases that the performance of deep learning methods is weakened when applied to different distributions Beery et al. [2018], Taori et al. [2020]. Among them, the $\mathcal{H}\Delta\mathcal{H}$ -divergence is proposed to measure the distance of error risk of two distinct distributions Ben-David et al. [2010]. Studies have been conducted to address OOD generalization issues Arjovsky et al. [2020], Ahuja et al. [2020], Gulrajani and Lopez-Paz [2020], Miller et al. [2021], Abbe et al. [2023], Chen et al. [2023]. One important branch of work aims to find invariant causal mechanisms across domains, inspired by the invariance principle from causality Arjovsky et al. [2020], Peters et al. [2016], Suter et al. [2019], Ahuja et al. [2020, 2022a], Chen et al. [2023]. Additionally, some studies incorporate SCM when analyzing the OOD problem Robey et al. [2021], Wald et al. [2021], Li et al. [2024]; a detailed comparison with them is provided in Section J. Vision-language pre-trained models, such as CLIP Radford et al. [2021], exhibit impressive performance across various domains. However, recent works emphasize that adapting CLIP with task-specific data often comes at the cost of OOD generalization ability Shu et al. [2023], Gao et al. [2023], Pham et al. [2023]. In our investigation of the invariant causal mechanisms of CLIP, we theoretically demonstrate that our method exhibits superior OOD generalization ability. We also provide a detailed analysis with some prior works in Section J.

3 Theoretical Analysis

3.1 Problem Setting

Before we start, note that the definition of all notations is provided in Appendix A. We begin by revisiting the framework for CLIP, as introduced by Radford et al. [2021]. Let $x \in \mathcal{X}$ represent an arbitrary image, and $t \in \mathcal{T}$ denote a text sequence describing this image. Here, \mathcal{X} denotes the image space, and \mathcal{T} represents the text space. CLIP comprises an image encoder $f_I : \mathcal{X} \rightarrow \hat{\mathcal{Z}}$ and a text encoder $f_T : \mathcal{T} \rightarrow \hat{\mathcal{Z}}$, which individually map the image and text into a shared embedding space $\hat{\mathcal{Z}} \subset \mathbb{R}^D$. Here, D signifies the dimensionality of the embedding space.

Next, we formalize the scenario in which CLIP is applied to the OOD generalization context. We consider supervised training data gathered from a set of environments E_{tr} : $\mathcal{D} = \{\mathcal{D}^e\}_{e \in E_{tr}}$, where $\mathcal{D}^e = \{\mathbf{x}_i^e, y_i^e\}_{i=1}^{N^e}$ represents the dataset from environment $e \in E_{tr}$. Here, N^e denotes the number of instances in environment e , $\mathbf{x}_i^e \in \mathcal{X}$ represents the image, and $y_i^e \in \mathcal{Y}$ represents the corresponding class label. Additionally, we assume that each class $c \in \mathcal{Y}$ can be described with a specific word $t_c \in \mathcal{T}$. OOD generalization aims to use the training data \mathcal{D} to construct a predictor $h : \mathcal{X} \rightarrow \mathcal{Y}$ that performs well across E_{all} , where $E_{tr} \subset E_{all}$. The OOD risk can be defined as:

$$R^{OOD}(h) = \max_{e \in E_{all}} R^e(h) = \max_{e \in E_{all}} \mathbb{E}_{(\mathbf{x}, y) \sim \mathcal{D}^e} [\mathbb{I}(h(\mathbf{x}) \neq y)], \quad (1)$$

where $\mathbb{I}(h(\mathbf{x}) \neq y)$ is the indicator function. It equals 0 if the prediction of h is correct and 1 if the prediction of h is wrong. Equation (1) implies that the OOD risk is defined as the maximum error risk across unseen environments. For CLIP, the predictor can be obtained in two ways: the linear-probe manner and the zero-shot manner.

The predictor with a linear probe requires training of a linear function parameterized by $W = [\mathbf{w}_1, \dots, \mathbf{w}_C] \in \mathbb{R}^{D \times C}$ and $b = [b_1, \dots, b_C] \in \mathbb{R}^C$ when the parameter of the image encoder f_I is frozen. Here, C denotes the total number of classes. Given the embedding of the image $f_I(\mathbf{x})$, the predictor $h : \hat{\mathcal{Z}} \rightarrow \mathcal{Y}$ is defined as a mapping from the embedding space to the label space as follows:

$$h(\hat{\mathbf{z}}) = \arg \max_{c \in \mathcal{Y}} \mathbf{w}_c^T \hat{\mathbf{z}} + b_c, \quad \text{where } \hat{\mathbf{z}} = f_I(\mathbf{x}). \quad (2)$$

In Equation (2), each \mathbf{w}_c and b_c corresponds to a $D - 1$ dimension hyperplane in the embedding space $\hat{\mathcal{Z}} \subset \mathbb{R}^D$ Mohri et al. [2018], where \mathbf{w}_c is the normal vector and b_c is a shifting scaler.

Another specific predictor for CLIP is the zero-shot prediction. The predictor requires no extra trainable parameters and can be directly performed with only the text description of the class label. For each class $c \in \mathcal{Y}$, a corresponding text prompt t_c is employed, where $t_c \in \mathcal{T}$, e.g., "a photo of a [CLASS]" where [CLASS] represents the name of class c . The text prompts of each class are then input into the text encoder f_T to obtain the class-specific text embedding $\hat{\mathbf{z}}_c = f_T(t_c)$. The predictor $h : \hat{\mathcal{Z}} \rightarrow \mathcal{Y}$ is therefore defined as:

$$h(\hat{\mathbf{z}}) = \arg \max_{c \in \mathcal{Y}} \frac{\hat{\mathbf{z}}_c^T \hat{\mathbf{z}}}{\|\hat{\mathbf{z}}_c\| \|\hat{\mathbf{z}}\|}, \quad \text{where } \hat{\mathbf{z}} = f_I(\mathbf{x}), \hat{\mathbf{z}}_c = f_T(t_c). \quad (3)$$

Note that in Equation (3), the embedding of the text prompt has the same function as the \mathbf{w}_c in the linear probe, except the bias is set to zero.

The purpose of the two prediction methods is essentially the same. For the issue of OOD generalization, the essence of both methods is to find a decision boundary defined by \mathbf{w}_c for each class $c \in \mathcal{Y}$ using data \mathcal{D} from only the training domain E_{tr} , and this decision boundary should be applicable to unseen domains. However, in the next subsection, we demonstrate through experiments that this property is not satisfied.

3.2 Motivation Experiment

Following the protocol defined above, we report the prediction accuracy on different domains in the VLCS dataset Torralba and Efros [2011] and present the results in Table 1. The linear-probe evaluation is conducted using the *leave-one-out* protocol, where for a specific domain, the training is performed using data from all other domains.

Table 1: Zero-shot and linear-probe prediction results in the VLCS dataset. Where **C**, **L**, **S** and **V** represent different domains.

Algorithm	C	L	S	V	Avg
CLIP Zero-shot	99.9±0.0	70.1±0.0	73.5±0.0	86.1±0.0	82.4
CLIP Linear-probe	93.7±0.2	65.4±0.2	76.4±0.2	79.1±0.3	78.7

It is evident from the table that accuracy varies across different domains. Specifically, when performing prediction with both zero-shot and linear-probe manner, in the **L** domain, classification accuracy is notably lower compared to other domains. Consequently, according to Equation (1), the OOD risk of CLIP is high, indicating the unsatisfactory OOD generalization ability of CLIP.

3.3 Causal Analysis

To further investigate the reasons behind CLIP’s unsatisfactory OOD generalization, we model both the data-generating and prediction processes using a Structural Causal Model (SCM), represented by Directed Acyclic Graphs (DAG) Glymour et al. [2016]. As illustrated in Figure 1, Figure 1(a) depicts the data-generating process, while Figure 1(b) outlines the prediction process.

Let $X \sim P(X)$ be the random variable representing images defined on \mathcal{X} , and let Y be the random variable representing class labels defined on \mathcal{Y} . Additionally, let $Z_{inv} \sim P(Z_{inv})$ and $Z_{var} \sim P(Z_{var})$ be the random variables representing invariant and variant latent factors, defined on \mathcal{Z}_{inv} and \mathcal{Z}_{var} respectively. Z_{inv} denotes the invariant latent factors that do not depend on the environment, while Z_{var} denotes the variant latent factors that depend on the environment. The joint space of the latent factors is defined

as $\mathcal{Z} = \mathcal{Z}_{inv} \times \mathcal{Z}_{var}$. We assume the independence of invariant and variant factors, meaning that the supports of \mathcal{Z}_{inv} and \mathcal{Z}_{var} are orthogonal. Additionally, we introduce a selection variable $E \sim P(E)$ defined on E_{all} to denote the environment, i.e., the domain Pearl and Bareinboim [2014]. The causal mechanism refers to the method of computationally deriving one variable from its parent nodes according to the SCM. For a detailed background on causality, including the definition of SCM and the selection variable E , refer to Appendix B.

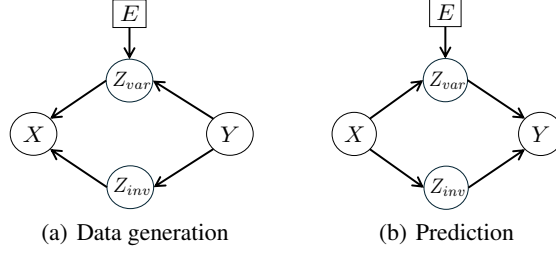


Figure 1: The SCM of both the data-generating process and prediction process of CLIP. The square denotes the selection variable, see Appendix B for details.

The SCM depicting the data-generating process is illustrated in Figure 1(a). In this SCM, the edge $E \rightarrow Z_{var}$ indicates that Z_{var} is influenced by the environment E . The edges $Z_{inv} \rightarrow X$ and the edge $Z_{var} \rightarrow X$ denote that the image can be generated by latent factors. We assume the generating process to be an injective function, specifically, $x = g(z)$, $z = [z_{inv}, z_{var}]$, $g : \mathcal{X} \rightarrow \mathcal{Z}$, $z \sim P(Z)$. The edge $Z_{inv} \leftarrow Y$ and the edge $Z_{var} \leftarrow Y$ suggest that the label can determine the value of the latent factors; for example, humans have 2 arms and 2 legs, cats have 1 tails, etc.

In the context of prediction tasks, the SCM depicting the prediction process is presented in Figure 1(b). Here, the edges $X \rightarrow Z_{var}$ and $X \rightarrow Z_{inv}$ signify the representation learning processes. For analytical convenience, we adopt an idealized assumption where the image encoder can function as the inverse process of data generation Bengio et al. [2014], Schölkopf et al. [2021], Zimmermann et al. [2022]. Specifically, for every $x \sim P(X)$, we denote $f(x) = z$, where $z = [z_{inv}, z_{var}]$, with $z_{inv} \sim P(Z_{inv})$ and $z_{var} \sim P(Z_{var})$. The edges $Z_{var} \rightarrow Y$ and $Z_{inv} \rightarrow Y$ are determined by the function h as defined in Equation (2) or Equation (3).

From SCM in Figure 1(b), we observe the following. Firstly, since Z_{var} and Z_{inv} serve as intermediate variables / nodes between X and Y , X and Y are conditionally independent given Z_{var} and Z_{inv} , denoted as $(Y \perp X | Z_{var}, Z_{inv})$ Pearl [2009]. Therefore, the process of predicting Y from X , $P(Y|X)$, can be accomplished jointly through Z_{var} and Z_{inv} , expressed as $P(Y|X) = P(Y|Z_{var}, Z_{inv})$. We provide an example of a multi-class classification task in Figure 2(a). From the figure, it can be observed that the optimal decision boundary’s normal vector w estimated with training data depends on both Z_{var} and Z_{inv} . When the environment remains unchanged, the distribution of X , Z_{var} , Z_{inv} , Y remains unchanged, allowing it to correctly perform classification on test data.

However, when the environment changes to a new environment $e^* \in E_{all}$, the presence of the edge $E \rightarrow Z_{var}$ leads to a change in the distribution of Z_{var} to Z_{var}^* . Consequently, due to the existence of the edge $Z_{var} \rightarrow X$ in the generation process of Figure 1(a), the distribution of images also changes. Consider the example in Figure 2(a), the classifier is tested on another environment e^* . Since in Figure 2(a), the prediction depends on both Z_{var} and Z_{inv} , a change of Z_{var} might lead to incorrect prediction in e^* , as shown in Figure 2(b).

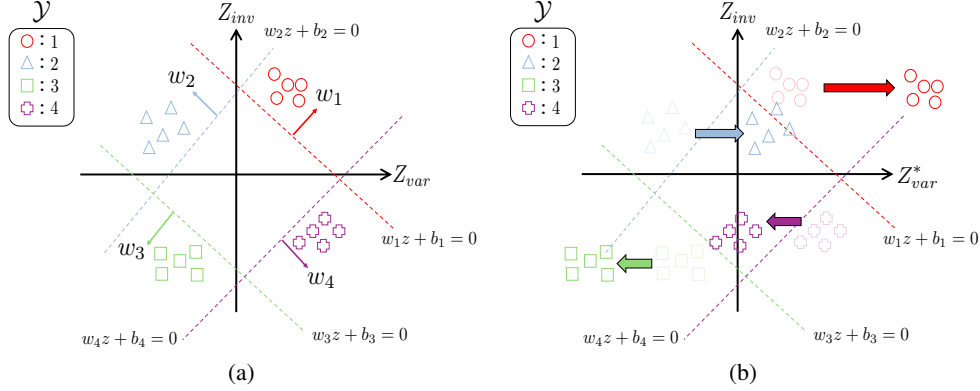


Figure 2: An example of a classifier defined on $\mathcal{Z} = \mathcal{Z}_{inv} \times \mathcal{Z}_{var}$ when applied to different environments, where the dashed lines represent the decision boundaries of specific classes and solid arrows depict the normal vectors of these boundaries. \mathcal{Y} is the set of labels. (a) illustrates an example of a classifier that is trained and tested in the same environment. (b) demonstrates applying the classifier from (a) to another environment $E = e^*$. The change in E only affects the distribution of Z_{var} .

Under what circumstances can we compute the prediction of Y through X under environment e^* ? To answer this question, we present the following theorem, which provides a causal mechanism for predicting Y through X under any environment E .

Theorem 3.1. *Let the distribution $P^*(\cdot) := P(\cdot|E = e^*)$ be the distribution on the test environment $E = e^*$. The causal mechanism $P^*(Y|X)$ can be computed with:*

$$P^*(Y|X) = \sum_{Z_{var}} \sum_{Z_{inv}} P(Y|Z_{var}, Z_{inv}) P(Z_{inv}|X) P^*(Z_{var}|X). \quad (4)$$

The detailed proof is provided in Appendix C. Since we assume the mapping from \mathcal{X} to \mathcal{Z} to be injective, the representation learning process $P(Z_{inv}|X)$ and $P^*(Z_{var}|X)$ are deterministic. Therefore, in a classification example, a specific probability $p^*(y|x)$ can be estimated using the softmax function as:

$$p^*(y|x) = \frac{\exp(\mathbf{z}^T \mathbf{w}_y)}{\sum_{c \in \mathcal{Y}} \exp(\mathbf{z}^T \mathbf{w}_c)} = \frac{\exp(\mathbf{z}_{inv}^T \mathbf{w}_{y,inv}) \cdot \exp(\mathbf{z}_{var}^{*T} \mathbf{w}_{y,var}^*)}{\sum_{c \in \mathcal{Y}} \exp(\mathbf{z}_{inv}^T \mathbf{w}_{c,inv}) \exp(\mathbf{z}_{var}^{*T} \mathbf{w}_{c,var}^*)}. \quad (5)$$

Here, $\mathbf{z} = [\mathbf{z}_{inv}, \mathbf{z}_{var}^*]$, $\mathbf{w}_c \in W$, and $\mathbf{w}_c = [\mathbf{w}_{c,inv}, \mathbf{w}_{c,var}^*]$. The optimal classifier on $E = e^*$ is composed of the invariant part $\mathbf{w}_{c,inv}$ and the variant part $\mathbf{w}_{c,var}^*$. While the invariant part can be trained with known environments E_{tr} , obtaining the variant part requires knowledge of the distribution of Z_{var} in the test environment e^* . However, in OOD scenarios, we lack access to the distribution of Z_{var} in e^* , leading to the failure of the learned classifier in E_{tr} when applied to unseen environments, as depicted in Figure 2(b). This raises the question of whether we can directly learn a classifier on the invariant factors and how well it performs in OOD scenarios. In the next sub-section, we analyze the OOD risk of the invariant predictor and regular predictor theoretically.

3.4 OOD Generalization Analysis

We consider the case where the representation learning stage is fixed. In this case, two types of predictors are learned in the training environment E_{tr} : the invariant predictor and the regular predictor. The invariant predictor operates on the latent factors $\mathbf{z}_{inv} \in \mathcal{Z}_{inv} \subset \mathbb{R}^{D_{inv}}$, while the regular predictor operates on the latent factors $\mathbf{z}_{var} \in \mathcal{Z}_{var} \subset \mathbb{R}^{D_{var}}$, $\mathbf{z} \in \mathcal{Z} \subset \mathbb{R}^D$, where $D_{inv} + D_{var} = D$. We can define the hypothesis \mathcal{H}_{inv} of invariant predictor as:

$$\mathcal{H}_{inv} = \{(\mathbf{z}_{inv}, y) \in \mathcal{Z}_{inv} \times \mathcal{Y} \mapsto \arg \max_{c \in \mathcal{Y}} \mathbf{w}_{c,inv}^T \mathbf{z}_{inv} + b_c : \mathbf{w}_{c,inv} \in \mathbb{R}^{D_{inv}}, b \in \mathbb{R}\}, \quad (6)$$

where $\mathbf{w}_{c,inv}$ and b_c are learnable parameters. Similarly, we can define the hypothesis \mathcal{H} of regular predictor as:

$$\mathcal{H} = \{(\mathbf{z}, y) \in \mathcal{Z} \times \mathcal{Y} \mapsto \arg \max_{c \in \mathcal{Y}} \mathbf{w}_c^T \mathbf{z} + b_c : \mathbf{w}_c \in \mathbb{R}^D, b \in \mathbb{R}\}, \quad (7)$$

where w_c^T and b_c are learnable parameters. Let the empirical risk on $e \in E_{tr}$ be $\hat{R}^e(h_{inv}) = \sum_{(\mathbf{x}, y) \in \mathcal{D}^e, \mathbf{z}_{inv} = f_{inv}^I(\mathbf{x})} \mathbb{I}(h(\mathbf{z}_{inv}) \neq y)$, where f_{inv}^I represents the path from $X \rightarrow Z_{inv}$ in SCM. The total empirical risk on all training environments $\hat{R}_{tr}(h_{inv})$ can be compute as $\hat{R}_{tr}(h_{inv}) = \sum_{e \in E_{tr}} \hat{R}^e(h_{inv})$. According to prior works Mohri et al. [2018], the generalization risk of $h_{inv} \in \mathcal{H}_{inv}$ on E_{tr} can be bounded with the Rademacher complexity $\mathfrak{R}(\mathcal{H}_{inv})$ of \mathcal{H}_{inv} . The Rademacher complexity represents a measure of the complexity of the hypothesis space. For any $\delta > 0$, with probability at least $1 - \delta$ over training samples of size N , we can bound the generalization risk as follows:

$$R_{tr}(h_{inv}) \leq \hat{R}_{tr}(h_{inv}) + \mathfrak{R}(\mathcal{H}_{inv}) + \sqrt{\frac{\log \frac{1}{\delta}}{2N}}. \quad (8)$$

Similarly, the generalization risk of regular predictor $h \in \mathcal{H}$ can be bounded with:

$$R_{tr}(h) \leq \hat{R}_{tr}(h) + \mathfrak{R}(\mathcal{H}) + \sqrt{\frac{\log \frac{1}{\delta}}{2N}}. \quad (9)$$

To measure the OOD risk of both invariant and regular predictor, we first define the distribution in training environments as P . We also define the distribution on some test environments $e^* \in E_{all}, e^* \notin E_{tr}$ as P^* . Let $R_{tr}(h, h') = \mathbb{E}_{z \sim P(z)}(\ell(h(z), h'(z)))$ be the expected disagreement between two hypotheses $h, h' \in \mathcal{H}$, where ℓ is some loss function (e.g. cross-entropy loss). This represents a measure of how much two hypotheses disagree with each other on the training distribution. We use $\mathcal{H}\Delta\mathcal{H}$ -divergence Ben-David et al. [2010], Chuang et al. [2020] to measure whether there is any pair of hypotheses whose risk differs significantly between P and P^* .

Definition 3.2. ($\mathcal{H}\Delta\mathcal{H}$ -divergence Ben-David et al. [2010]) Given two distribution P and P^* , and a hypothesis class \mathcal{H} , the $\mathcal{H}\Delta\mathcal{H}$ -divergence between P and P^* is:

$$d_{\mathcal{H}\Delta\mathcal{H}}(P, P^*) := \sup_{h, h' \in \mathcal{H}} |R_{tr}(h, h') - R^*(h, h')|. \quad (10)$$

Note that the $d_{\mathcal{H}_{inv}\Delta\mathcal{H}_{inv}}(P, P^*)$ of invariant hypothesis class \mathcal{H}_{inv} is zero. This is because the distributions $P(Z_{inv})$ and $P^*(Z_{inv})$ are equal. But it does not hold for the regular hypothesis \mathcal{H} . We now prove that the OOD risk of the invariant predictor is lower than that of the regular predictor under certain conditions.

Theorem 3.3. *Let the empirical risk gap $\hat{R}_{tr}(h) - \hat{R}_{tr}(h_{inv}) = \mathcal{C}_1$, and the Rademacher complexity gap $\mathfrak{R}(\mathcal{H}) - \mathfrak{R}(\mathcal{H}_{inv}) = \mathcal{C}_2$. If $d_{\mathcal{H}\Delta\mathcal{H}}(P, P^*) > \mathcal{C}_1 - \mathcal{C}_2, \forall e^* \in E_{all}, e^* \notin E_{tr}$. Then, the OOD risk of the invariant predictor is lower than that of the regular predictor:*

$$R^{\text{OOD}}(h_{inv}) < R^{\text{OOD}}(h), \quad \forall h_{inv} \in \mathcal{H}_{inv}, h \in \mathcal{H}. \quad (11)$$

Theorem 3.3 states that if the divergence between the training environment and test divergence is larger than some constant, the OOD risk of the invariant predictor is smaller than the regular predictor.

In practice, when the true distribution P^* is unknown, the divergence between the training and test environments is often significant. To ensure a smaller OOD risk, one only needs to ensure that the invariant predictor has low empirical risk. Next, we provide the methodology for designing such a predictor for CLIP, especially in the zero-shot setting.

4 Methodology

To acquire an invariant predictor, prior works have explored learning predictors that are invariant across domains Arjovsky et al. [2019], Ahuja et al. [2022a], Yang et al. [2023]. However, these approaches require training with labeled data, which limits their applicability to scenarios where the test labels are seen during training. In many cases, labeled data may not be available. On the other hand, if we can determine the invariant space \mathcal{Z}_{inv} , we can directly perform invariant zero-shot prediction by mapping the text embedding to \mathcal{Z}_{inv} . This challenge mirrors the well-established problem of identifying the latent factors responsible for generating the data Schölkopf et al. [2021], Hyvärinen and Oja [2000].

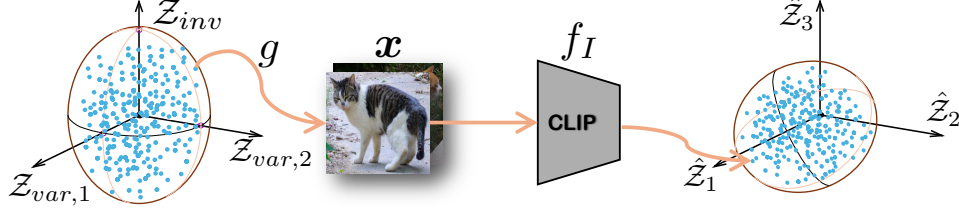


Figure 3: A graphical illustration of Proposition 4.1. In the figure, suppose that the image x is generated from the latent space $\mathcal{Z} = \mathcal{Z}_{inv} \times \mathcal{Z}_{var,1} \times \mathcal{Z}_{var,2}$ with $g : \mathcal{Z} \rightarrow \mathcal{X}$. Proposition 4.1 implies that the output of the CLIP encoder $\hat{\mathcal{Z}} = \hat{\mathcal{Z}}_1 \times \hat{\mathcal{Z}}_2 \times \hat{\mathcal{Z}}_3$ is a invertible linear transformation of the latent space \mathcal{Z} .

The identification of latent factors can be considered as learning an encoder function $f : \mathcal{X} \rightarrow \mathcal{Z}$ which inverts the data-generating process of $g : \mathcal{Z} \rightarrow \mathcal{X}$. However, due to the absence of additional knowledge about the latent factors, we can only prove that, under a specific constraint, the encoder function's output is a linear transformation of the true latent. Specifically, for $x = g(z), z \sim P(Z)$, $f(x) = Az$, where $A \in \mathbb{R}^{D \times D}$ is an invertible matrix.

Proposition 4.1. *Consider the data generating process of CLIP as an injective function, where $x = g(z), z \sim P(Z)$. Suppose there exists an ideal encoder $f_{I^*} : \mathcal{X} \rightarrow \mathcal{Z}$, such that $f_{I^*}(x) = g^{-1}(x) = z$. Here I^* is the ideal parameter of the image encoder, T^* is the ideal parameter of the text encoder. Let $\mathcal{Z} \subset \mathbb{R}^D$, if $|\mathcal{T}| \geq (1 + \sqrt{1 + 8D})/2$ in E_{tr} , and the loss function is minimized, where the prediction results of the learned encoder f_I is the same as the ideal encoder f_{I^*} . Then the learned encoder $f_I(x)$ identifies the latent factor \mathcal{Z} up to an invertible linear transformation A , i.e. $f_I(x) = Az$.*

The proof is illustrated in Appendix E. Figure 3 provides a graphical explanation. This conclusion is a commonly recognized result from a series of works Roeder et al. [2021], Ahuja et al. [2022b], Hyvarinen and Morioka [2016], Zimmermann et al. [2022], and Proposition 4.1 provides a proof of it in our scenario. CLIP can be considered satisfying Proposition 4.1 because it was trained on a dataset of 400 million (image, text) pairs collected from the Internet which is much higher than $(1 + \sqrt{1 + 8D})/2$, where D usually takes no more than 2048 Radford et al. [2021]. However, since the mixing matrix A is arbitrary, the linear identifiability of latent factors alone is insufficient to ensure identifying \mathcal{Z}_{inv} .

Note that the aforementioned analyses are all based on observational data. The causality seeks to answer questions related to interventions, such as predicting the model's response when changing a real-world image to a sketched painting Bareinboim et al. [2022]. This involves intervening on factors like background color and texture. The operation, known as a *do*-intervention, alters latent factors, and the resulting distribution of \mathcal{Z} differs from the observational distribution $P(Z)$. Formally, a *do*-intervention sets the value of a specific latent factor to a fixed value $do(z_i) = z_i^\dagger$, while the distribution of other latent factors is $P^{do(z_i)}(Z)$. The distribution of the interventional data is $P^{do(z_i)}(X)$ supported on $\mathcal{X}^{do(z_i)}$. Next, we demonstrate that by intervening on a specific latent factor, denoted as z_i , such that for all $x \in \mathcal{X}^{do(z_i)}$, the k -th output of the encoder remains a fixed value, the encoder can identify the corresponding intervened latent factor up to shift and scaling.

Theorem 4.2. *Consider observational data generated from an injective mapping $g : \mathcal{Z} \rightarrow \mathcal{X}$, where the latent factors \mathcal{Z} follow a distribution $P(Z)$ supported on \mathcal{Z} . If a *do*-intervention is applied to the i -th latent factor z_i to take a fixed value, with the distribution of other latent factors denoted as $P^{do(z_i)}(Z)$, the resulting distribution of the interventional data is denoted as $P^{do(z_i)}(X)$. Suppose that an encoder f_I satisfies Proposition 4.1, and the output of the k^{th} component of the encoder is*

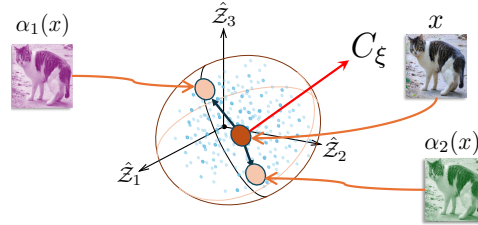


Figure 4: Graphical illustration of Equation (12). Minimizing Equation (12) is equivalent to finding the principle components of $\hat{\mathcal{Z}}$ which is invariant to any data augmentations α_j , i.e. finding the normal vector of the \mathcal{Z}_{var} space.

Table 2: Accuracy on VLCS dataset.

Algorithm	Backbone	C	L	S	V	Avg
ERM	R50	97.7±0.4	64.3±0.9	73.4±0.5	74.6±1.3	77.5
IRM Arjovsky et al. [2020]	R50	98.6±0.1	64.9±0.9	73.4±0.6	77.3±0.9	78.5
GroupDRO Sagawa* et al. [2019]	R50	97.3±0.3	63.4±0.9	69.5±0.8	76.7±0.7	76.7
Mixup Yan et al. [2020]	R50	98.3±0.6	64.8±1.0	72.1±0.5	74.3±0.8	77.4
MMD Li et al. [2018]	R50	97.7±0.1	64.0±1.1	72.8±0.2	75.3±3.3	77.5
DANN Ganin et al. [2016]	R50	99.0±0.3	65.1±1.4	73.1±0.3	77.2±0.6	78.6
ARM Zhang et al. [2021]	R50	98.7±0.2	63.6±0.7	71.3±1.2	76.7±0.6	77.6
MBDG Robey et al. [2021]	R50	98.3	68.1	68.8	76.3	77.9
CLIP Linear-probe	R50	98.1±0.7	63.8±0.8	79.8±0.7	84.5±1.0	81.5
CLIP-ICM Linear-probe	R50	99.2±0.1	69.9±0.3	80.5±0.3	89.5±0.9	84.8
CLIPOOD Shu et al. [2023]	ViT-B	97.5±0.6	68.3±0.5	83.9±0.9	88.7±1.0	84.6
CLIP Linear-probe	ViT-B	93.7±0.2	65.4±0.2	76.4±0.2	79.1±0.3	78.7
CLIP-ICM Linear-probe	ViT-B	98.8±0.3	72.7±0.8	86.4±0.9	87.9±0.9	86.5
CLIP Zero-shot	R50	99.2±0.0	69.5±0.0	69.8±0.0	84.9±0.0	80.9
CLIP-ICM Zero-shot	R50	99.4±0.4	71.8±0.8	71.7±0.8	85.3±1.0	82.1
CLIP Zero-shot	ViT-B	99.9±0.0	70.1±0.0	73.5±0.0	86.1±0.0	82.4
CLIP-ICM Zero-shot	ViT-B	100.0±0.0	74.7±0.4	74.5±0.4	87.1±0.7	84.1

Table 3: Accuracy on TerraIncognita dataset.

Algorithm	Backbone	L100	L38	L43	L46	Avg
ERM	R50	49.8±4.4	42.1±1.4	56.9±1.8	35.7±3.9	46.1
IRM Arjovsky et al. [2020]	R50	54.6±1.3	39.8±1.9	56.2±1.8	39.6±0.8	47.6
GroupDRO Sagawa* et al. [2019]	R50	41.2±0.7	38.6±2.1	56.7±0.9	36.4±2.1	43.2
Mixup Yan et al. [2020]	R50	59.6±2.0	42.2±1.4	55.9±0.8	33.9±1.4	47.9
MMD Li et al. [2018]	R50	41.9±3.0	34.8±1.0	57.0±1.9	35.2±1.8	42.2
DANN Ganin et al. [2016]	R50	51.1±3.5	40.6±0.6	57.4±0.5	37.7±1.8	46.7
ARM Zhang et al. [2021]	R50	49.3±0.7	38.3±2.4	55.8±0.8	38.7±1.3	45.5
CLIP Linear-probe	R50	52.0±1.0	34.4±0.6	56.1±0.9	32.8±0.2	44.1
CLIP-ICM Linear-probe	R50	64.1±0.4	46.5±0.7	61.1±0.6	42.8±0.4	53.6
CLIPOOD Shu et al. [2023]	ViT-B	74.6±0.3	57.3±0.5	59.1±0.9	47.7±0.9	59.7
CLIP Linear-probe	ViT-B	73.6±0.5	58.3±0.7	61.0±0.1	47.8±1.0	60.2
CLIP-ICM Linear-probe	ViT-B	78.7±0.5	60.2±0.9	66.0±0.8	52.4±0.1	64.3
CLIP Zero-shot	R50	7.7±0.0	14.8±0.0	32.4±0.0	20.9±0.0	19.0
CLIP-ICM Zero-shot	R50	38.8±0.4	33.6±0.6	33.6±0.1	30.1±0.7	34.0
CLIP Zero-shot	ViT-B	52.0±0.0	20.4±0.0	32.8±0.0	31.6±0.0	34.2
CLIP-ICM Zero-shot	ViT-B	59.3±0.4	46.2±0.4	52.4±0.7	41.6±0.8	49.9

required to take a fixed value $f_I(\mathbf{x})[k] = z_i^\dagger$ for all $\mathbf{x} \in \mathcal{X}^{do(z_i)}$. Then, the encoder identifies the intervened latent z_i up to a shift and scaling, i.e., $f_I(\mathbf{x})[k] = a_i z_i + b_i$, where $a_i \in \mathbb{R}$ and $b_i \in \mathbb{R}$.

The proof is detailed in Appendix F. Theorem 4.2 provides a condition under which \mathcal{Z}_{inv} can be identified. Subsequently, leveraging the condition outlined in Theorem 4.2, we introduce a straightforward and efficient algorithm named CLIP-ICM. This algorithm functions as a post-processing step for the output of the CLIP encoders and is designed to meet the requirements of the condition specified in Theorem 4.2. We perform a set of interventions by utilizing data augmentation techniques on the raw image. For an image sample with different augmentations, it can be regarded that only \mathcal{Z}_{var} is changed while the \mathcal{Z}_{inv} remains fixed. Therefore, according to Proposition 4.1 and Theorem 4.2, we can estimate a linear matrix $C_\xi \in \mathbb{R}^{D_{inv} \times D}$ such that $C_\xi \hat{\mathcal{Z}}$ can identify the invariant subspace \mathcal{Z}_{inv} .

From a principle component analysis perspective, C_ξ should possess two essential properties Krogh and Hertz [1991]: (1) The projected representation through C_ξ should contain as much information about the original representation $f_I(\mathbf{x})$ as possible. This can be considered as minimizing the empirical risk according to Theorem 3.3. (2) The projected representation through C_ξ should be invariant to any intervention on \mathcal{Z}_{var} , which is equivalent to finding the orthogonal subspace of \mathcal{Z}_{var} . This process can be considered as satisfying the constraint in Theorem 4.2 to identify \mathcal{Z}_{inv} . Therefore, the objective to acquire C_ξ is:

$$\min_{C_\xi} \|\hat{\mathcal{Z}} - \hat{\mathcal{Z}}^T C_\xi^T C_\xi\|_2^2 + \lambda \sum_{j \in K} \|C_\xi(\hat{\mathcal{Z}} - f_I(\alpha_j(\mathbf{x})))\|_2^2 \quad s.t. \quad \text{rank}(\hat{\mathcal{Z}}^T C_\xi^T C_\xi) \leq D_{inv}, \quad (12)$$

where $\hat{\mathcal{Z}} = [\hat{z}_1, \dots, \hat{z}_N]^T$, λ is a hyperparameter, j is the type of data augmentation, K is the total types of data augmentation, α_j is the j -th data augmentation. **Note that the objective Equation (12) doesn't require any labeled data.**

To perform the invariant prediction with the estimated C_ξ in a zero-shot manner, for any test image \mathbf{x} with fixed prompt \mathbf{t} , such as "a photo of a [CLASS]". We only need to apply C_ξ to both the text embedding $f_T(\mathbf{t})$ and the image embedding $f_I(\mathbf{x})$ and perform zero-shot prediction of Equation (3) with the projected embedding. To perform invariant prediction in a linear-probe manner, we only need to train a classifier on the projected image embedding and perform prediction with Equation (2).

5 Experiment

To validate the effectiveness of the proposed CLIP-ICM in OOD scenarios, we conduct experiments on the well-known benchmark DomainBed Gulrajani and Lopez-Paz [2020]. Specifically, we select three datasets from DomainBed, namely VLCS Fang et al. [2013], TerraIncognita Beery et al. [2018], and DomainNet Peng et al. [2019]. We provide additional results on the Office-Home Venkateswara et al. [2017] and PCAS Li et al. [2017] datasets in Appendix H. The implementation details are outlined in Appendix G. Furthermore, we conduct ablation studies to investigate the impact of the hyper-parameters and data augmentation choices on our model's performance in Appendix K. Finally, we analyze the effect of zero-shot prediction with domain prompts in Appendix L.

Results. The classification results of CLIP-ICM on VLCS, TerraIncognita, and DomainNet are illustrated in Table 2, Table 3 and Table 4 respectively. Results without error bars are from the original paper, where they didn't provide it. It is clear from the tables that the CLIP-ICM significantly improves the performance of CLIP in both zero-shot and linear-probe manner. Specifically, in the

Table 4: Accuracy on DomainNet dataset.

Algorithm	Backbone	CLIPART	INFOGRAPH	PAINTING	QUICKDRAW	REAL	SKETCH	Avg
ERM	R50	58.1±0.3	18.8±0.3	46.7±0.3	12.2±0.4	59.6±0.1	49.8±0.4	40.9
IRM Arjovsky et al. [2020]	R50	48.5±2.8	15.0±1.5	38.3±4.3	10.9±0.5	48.2±5.2	42.3±3.1	33.9
GroupDRO Sagawa* et al. [2019]	R50	47.2±0.5	17.5±0.4	33.8±0.5	9.3±0.3	51.6±0.4	40.1±0.6	33.3
Mixup Yan et al. [2020]	R50	55.7±0.3	18.5±0.5	44.3±0.5	12.5±0.4	55.8±0.3	48.2±0.5	39.2
MMD Li et al. [2018]	R50	32.1±13.3	11.0±4.6	26.8±11.3	8.7±2.1	32.7±13.8	28.9±11.9	23.4
DANN Ganin et al. [2016]	R50	53.1±0.2	18.3±0.1	44.2±0.7	11.8±0.1	55.5±0.4	46.8±0.6	38.3
ARM Zhang et al. [2021]	R50	49.7±0.3	16.3±0.5	40.9±1.1	9.4±0.1	53.4±0.4	43.5±0.4	35.5
CLIP Linear-probe	R50	59.2±0.1	38.6±0.9	54.1±0.7	8.2±0.7	56.4±0.7	39.6±0.7	42.6
CLIP-ICM Linear-probe	R50	63.1±0.1	50.1±0.2	66.2±1.0	19.7±0.3	83.8±0.4	63.2±0.3	57.8
CLIPOOD Shu et al. [2023]	ViT-B	77.6	54.7	72.5	20.7	85.7	69.9	63.5
CLIP Linear-probe	ViT-B	73.9±0.5	40.2±0.5	62.1±0.2	15.1±0.3	76.9±0.1	62.0±0.7	55.0
CLIP-ICM Linear-probe	ViT-B	78.6±0.2	55.6±0.2	72.9±0.6	22.1±0.7	86.1±0.3	68.5±0.3	64.0
CLIP Zero-shot	R50	53.1±0.0	39.2±0.0	52.9±0.0	5.7±0.0	76.7±0.0	48.0±0.0	45.9
CLIP-ICM Zero-shot	R50	58.0±0.1	42.3±0.5	54.4±0.2	12.8±0.7	78.2±0.1	49.6±0.2	49.2
CLIP Zero-shot	ViT-B	70.2±0.0	46.6±0.0	65.0±0.0	13.7±0.0	82.9±0.0	62.7±0.0	56.8
CLIP-ICM Zero-shot	ViT-B	77.1±0.5	51.8±0.5	67.9±1.0	16.7±0.3	82.9±0.8	66.9±0.2	60.5

linear probe of the VLCS dataset, CLIP-ICM shows a notable improvement of **10.0%** in the **S** domain. Similarly, in the zero-shot setting of the TerraIncognita dataset, CLIP-ICM achieves an impressive improvement of **31.1%** in the **L100** domain. Moreover, the accuracy of CLIP-ICM is consistently improved across all domains, surpassing other state-of-the-art domain generalization methods.

6 Conclusion

In our work, we observe the unsatisfactory performance of CLIP in OOD scenarios. Through theoretical analysis, we demonstrate that the invariant predictor can achieve lower OOD generalization risk if certain requirements are met, which raises two challenges including the identifiability of the invariant factors and an invariant predictor with lower empirical risks. Guided by the theoretical conclusions, we propose CLIP-ICM, which leverages interventional data through data augmentation to identify the invariant subspace that maintains the maximum information and performs invariant prediction in both zero-shot and linear-probe manner. Experimental results demonstrate the superior results of CLIP-ICM on the Domainbed Benchmark in comparison to existing methods.

Limitations. While CLIP-ICM has shown promising results, its evaluation is limited to classification tasks. However, our analysis has broader implications and can be applied to various real-world scenarios. In future research, we will continue to explore its potential applications.

Broader Impact. Our work takes a step towards achieving general artificial intelligence by introducing the invariant causal mechanism into vision-language models. This innovation has significant societal implications, as it can potentially promote interpretable machine learning.

References

- Emmanuel Abbe, Samy Bengio, Aryo Lotfi, and Kevin Rizk. Generalization on the Unseen, Logic Reasoning and Degree Curriculum. In *Proceedings of the 40th International Conference on Machine Learning*, pages 31–60. PMLR, July 2023. ISSN: 2640-3498.
- Kartik Ahuja, Karthikeyan Shanmugam, Kush Varshney, and Amit Dhurandhar. Invariant Risk Minimization Games. In *Proceedings of the 37th International Conference on Machine Learning*, pages 145–155. PMLR, November 2020. ISSN: 2640-3498.
- Kartik Ahuja, Ethan Caballero, Dinghuai Zhang, Jean-Christophe Gagnon-Audet, Yoshua Bengio, Ioannis Mitliagkas, and Irina Rish. Invariance Principle Meets Information Bottleneck for Out-of-Distribution Generalization, November 2022a. arXiv:2106.06607 [cs, stat].
- Kartik Ahuja, Divyat Mahajan, Vasilis Syrgkanis, and Ioannis Mitliagkas. Towards efficient representation identification in supervised learning, April 2022b. arXiv:2204.04606 [cs, stat].
- Kartik Ahuja, Divyat Mahajan, Yixin Wang, and Yoshua Bengio. Interventional Causal Representation Learning. In *Proceedings of the 40th International Conference on Machine Learning*, pages 372–407. PMLR, July 2023. ISSN: 2640-3498.

- Martin Arjovsky, Léon Bottou, Ishaan Gulrajani, and David Lopez-Paz. Invariant risk minimization. *arXiv preprint arXiv:1907.02893*, 2019.
- Martin Arjovsky, Léon Bottou, Ishaan Gulrajani, and David Lopez-Paz. Invariant Risk Minimization, March 2020. arXiv:1907.02893 [cs, stat].
- Elias Bareinboim, Juan D. Correa, Duligur Ibeling, and Thomas Icard. On Pearl’s Hierarchy and the Foundations of Causal Inference. In Hector Geffner, Rina Dechter, and Joseph Y. Halpern, editors, *Probabilistic and Causal Inference*, pages 507–556. ACM, New York, NY, USA, 1 edition, February 2022. ISBN 978-1-4503-9586-1. doi: 10.1145/3501714.3501743.
- Sara Beery, Grant Van Horn, and Pietro Perona. Recognition in terra incognita. In *Proceedings of the European conference on computer vision (ECCV)*, pages 456–473, 2018.
- Shai Ben-David, John Blitzer, Koby Crammer, Alex Kulesza, Fernando Pereira, and Jennifer Wortman Vaughan. A theory of learning from different domains. *Machine learning*, 79:151–175, 2010.
- Yoshua Bengio, Aaron Courville, and Pascal Vincent. Representation Learning: A Review and New Perspectives, April 2014. arXiv:1206.5538 [cs].
- Christopher M. Bishop. Latent Variable Models. In Michael I. Jordan, editor, *Learning in Graphical Models*, pages 371–403. Springer Netherlands, Dordrecht, 1998. ISBN 978-94-010-6104-9 978-94-011-5014-9. doi: 10.1007/978-94-011-5014-9_13.
- Simon Buchholz, Goutham Rajendran, Elan Rosenfeld, Bryon Aragam, Bernhard Schölkopf, and Pradeep Ravikumar. Learning Linear Causal Representations from Interventions under General Nonlinear Mixing, December 2023. arXiv:2306.02235 [cs, math, stat].
- Ting Chen, Simon Kornblith, Mohammad Norouzi, and Geoffrey Hinton. A Simple Framework for Contrastive Learning of Visual Representations. In *Proceedings of the 37th International Conference on Machine Learning*, pages 1597–1607. PMLR, November 2020. ISSN: 2640-3498.
- Yongqiang Chen, Kaiwen Zhou, Yatao Bian, Binghui Xie, Bingzhe Wu, Yonggang Zhang, Ma Kaili, Han Yang, Peilin Zhao, Bo Han, and James Cheng. Pareto Invariant Risk Minimization: Towards Mitigating the Optimization Dilemma in Out-of-Distribution Generalization. February 2023.
- Ching-Yao Chuang, Antonio Torralba, and Stefanie Jegelka. Estimating generalization under distribution shifts via domain-invariant representations. In *International Conference on Machine Learning*, pages 1984–1994. PMLR, 2020.
- Mohamed Elhoseiny, Babak Saleh, and Ahmed Elgammal. Write a classifier: Zero-shot learning using purely textual descriptions. In *Proceedings of the IEEE International Conference on Computer Vision*, pages 2584–2591, 2013.
- Chen Fang, Ye Xu, and Daniel N Rockmore. Unbiased metric learning: On the utilization of multiple datasets and web images for softening bias. In *Proceedings of the IEEE International Conference on Computer Vision*, pages 1657–1664, 2013.
- Andrea Frome, Greg S. Corrado, Jon Shlens, Samy Bengio, Jeff Dean, Marc’Aurelio Ranzato, and Tomas Mikolov. Devise: A deep visual-semantic embedding model. *Advances in neural information processing systems*, 26, 2013.
- Yaroslav Ganin, Evgeniya Ustinova, Hana Ajakan, Pascal Germain, Hugo Larochelle, François Laviolette, Mario March, and Victor Lempitsky. Domain-adversarial training of neural networks. *Journal of machine learning research*, 17(59):1–35, 2016.
- Peng Gao, Shijie Geng, Renrui Zhang, Teli Ma, Rongyao Fang, Yongfeng Zhang, Hongsheng Li, and Yu Qiao. CLIP-Adapter: Better Vision-Language Models with Feature Adapters. *International Journal of Computer Vision*, September 2023. ISSN 0920-5691, 1573-1405. doi: 10.1007/s11263-023-01891-x.
- Madelyn Glymour, Judea Pearl, and Nicholas P. Jewell. *Causal Inference in Statistics: A Primer*. John Wiley & Sons, January 2016. ISBN 978-1-119-18686-1. Google-Books-ID: I0V2CwAAQBAJ.

- Ishaan Gulrajani and David Lopez-Paz. In Search of Lost Domain Generalization, July 2020. arXiv:2007.01434 [cs, stat].
- Aapo Hyvärinen and Hiroshi Morioka. Unsupervised feature extraction by time-contrastive learning and nonlinear ica. *Advances in neural information processing systems*, 29, 2016.
- Aapo Hyvärinen and Hiroshi Morioka. Nonlinear ICA of Temporally Dependent Stationary Sources. In *Proceedings of the 20th International Conference on Artificial Intelligence and Statistics*, pages 460–469. PMLR, April 2017. ISSN: 2640-3498.
- A. Hyvärinen and E. Oja. Independent component analysis: algorithms and applications. *Neural Networks*, 13(4):411–430, June 2000. ISSN 0893-6080. doi: 10.1016/S0893-6080(00)00026-5.
- Aapo Hyvärinen and Petteri Pajunen. Nonlinear independent component analysis: Existence and uniqueness results. *Neural Networks*, 12(3):429–439, April 1999. ISSN 0893-6080. doi: 10.1016/S0893-6080(98)00140-3.
- Chao Jia, Yinfei Yang, Ye Xia, Yi-Ting Chen, Zarana Parekh, Hieu Pham, Quoc Le, Yun-Hsuan Sung, Zhen Li, and Tom Duerig. Scaling up visual and vision-language representation learning with noisy text supervision. In *International conference on machine learning*, pages 4904–4916. PMLR, 2021.
- Oliver Kramer. Scikit-Learn. In *Machine Learning for Evolution Strategies*, volume 20, pages 45–53. Springer International Publishing, Cham, 2016. ISBN 978-3-319-33381-6 978-3-319-33383-0. doi: 10.1007/978-3-319-33383-0_5. Series Title: Studies in Big Data.
- Anders Krogh and John Hertz. A simple weight decay can improve generalization. *Advances in neural information processing systems*, 4, 1991.
- Julius Von Kügelgen, Yash Sharma, Luigi Gresele, Wieland Brendel, Bernhard Schölkopf, Michel Besserve, and Francesco Locatello. Self-Supervised Learning with Data Augmentations Provably Isolates Content from Style. November 2021.
- Sébastien Lachapelle, Pau Rodríguez López, Yash Sharma, Katie Everett, Rémi Le Priol, Alexandre Lacoste, and Simon Lacoste-Julien. Disentanglement via Mechanism Sparsity Regularization: A New Principle for Nonlinear ICA, February 2022. arXiv:2107.10098 [cs, stat].
- Da Li, Yongxin Yang, Yi-Zhe Song, and Timothy M Hospedales. Deeper, broader and artier domain generalization. In *Proceedings of the IEEE international conference on computer vision*, pages 5542–5550, 2017.
- Haoliang Li, Sinno Jialin Pan, Shiqi Wang, and Alex C Kot. Domain generalization with adversarial feature learning. In *Proceedings of the IEEE conference on computer vision and pattern recognition*, pages 5400–5409, 2018.
- Zijian Li, Ruichu Cai, Guangyi Chen, Boyang Sun, Zhifeng Hao, and Kun Zhang. Subspace identification for multi-source domain adaptation. *Advances in Neural Information Processing Systems*, 36, 2024.
- Francesco Locatello, Stefan Bauer, Mario Lucic, Gunnar Rätsch, Sylvain Gelly, Bernhard Schölkopf, and Olivier Bachem. Challenging Common Assumptions in the Unsupervised Learning of Disentangled Representations, June 2019. arXiv:1811.12359 [cs, stat].
- Francesco Locatello, Ben Poole, Gunnar Rätsch, Bernhard Schölkopf, Olivier Bachem, and Michael Tschannen. Weakly-supervised disentanglement without compromises. In *International Conference on Machine Learning*, pages 6348–6359. PMLR, 2020.
- John P. Miller, Rohan Taori, Aditi Raghunathan, Shiori Sagawa, Pang Wei Koh, Vaishaal Shankar, Percy Liang, Yair Carmon, and Ludwig Schmidt. Accuracy on the line: on the strong correlation between out-of-distribution and in-distribution generalization. In *International Conference on Machine Learning*, pages 7721–7735. PMLR, 2021.
- Mehryar Mohri, Afshin Rostamizadeh, and Ameet Talwalkar. *Foundations of machine learning*. MIT press, 2018.

- Mohammad Norouzi, Tomas Mikolov, Samy Bengio, Yoram Singer, Jonathon Shlens, Andrea Frome, Greg S. Corrado, and Jeffrey Dean. Zero-Shot Learning by Convex Combination of Semantic Embeddings, March 2014. arXiv:1312.5650 [cs].
- Judea Pearl. *Causality*. Cambridge university press, 2009.
- Judea Pearl and Elias Bareinboim. External Validity: From Do-Calculus to Transportability Across Populations. *Statistical Science*, 29(4):579–595, November 2014. ISSN 0883-4237, 2168-8745. doi: 10.1214/14-STS486. Publisher: Institute of Mathematical Statistics.
- Xingchao Peng, Qinxun Bai, Xide Xia, Zijun Huang, Kate Saenko, and Bo Wang. Moment matching for multi-source domain adaptation. In *Proceedings of the IEEE/CVF international conference on computer vision*, pages 1406–1415, 2019.
- Jonas Peters, Peter Bühlmann, and Nicolai Meinshausen. Causal Inference by using Invariant Prediction: Identification and Confidence Intervals. *Journal of the Royal Statistical Society Series B: Statistical Methodology*, 78(5):947–1012, November 2016. ISSN 1369-7412, 1467-9868. doi: 10.1111/rssb.12167.
- Hieu Pham, Zihang Dai, Golnaz Ghiasi, Kenji Kawaguchi, Hanxiao Liu, Adams Wei Yu, Jiahui Yu, Yi-Ting Chen, Minh-Thang Luong, Yonghui Wu, Mingxing Tan, and Quoc V. Le. Combined scaling for zero-shot transfer learning. *Neurocomputing*, 555:126658, October 2023. ISSN 09252312. doi: 10.1016/j.neucom.2023.126658.
- Alec Radford, Jong Wook Kim, Chris Hallacy, Aditya Ramesh, Gabriel Goh, Sandhini Agarwal, Girish Sastry, Amanda Askell, Pamela Mishkin, Jack Clark, Gretchen Krueger, and Ilya Sutskever. Learning Transferable Visual Models From Natural Language Supervision. In *Proceedings of the 38th International Conference on Machine Learning*, pages 8748–8763. PMLR, July 2021. ISSN: 2640-3498.
- Alexander Robey, George J. Pappas, and Hamed Hassani. Model-based domain generalization. *Advances in Neural Information Processing Systems*, 34:20210–20229, 2021.
- Geoffrey Roeder, Luke Metz, and Durk Kingma. On linear identifiability of learned representations. In *International Conference on Machine Learning*, pages 9030–9039. PMLR, 2021.
- Shiori Sagawa*, Pang Wei Koh*, Tatsunori B. Hashimoto, and Percy Liang. Distributionally Robust Neural Networks. December 2019.
- Bernhard Schölkopf, Dominik Janzing, Jonas Peters, Eleni Sgouritsa, Kun Zhang, and Joris Mooij. On Causal and Anticausal Learning, June 2012. arXiv:1206.6471 [cs, stat].
- Bernhard Schölkopf, Francesco Locatello, Stefan Bauer, Nan Rosemary Ke, Nal Kalchbrenner, Anirudh Goyal, and Yoshua Bengio. Toward Causal Representation Learning. *Proceedings of the IEEE*, 109(5):612–634, May 2021. ISSN 1558-2256. doi: 10.1109/JPROC.2021.3058954. Conference Name: Proceedings of the IEEE.
- Yang Shu, Xingzhuo Guo, Jialong Wu, Ximei Wang, Jianmin Wang, and Mingsheng Long. CLIPood: Generalizing CLIP to Out-of-Distributions, July 2023. arXiv:2302.00864 [cs].
- Richard Socher, Milind Ganjoo, Christopher D. Manning, and Andrew Ng. Zero-shot learning through cross-modal transfer. *Advances in neural information processing systems*, 26, 2013.
- Chandler Squires, Anna Seigal, Salil S. Bhate, and Caroline Uhler. Linear causal disentanglement via interventions. In *International Conference on Machine Learning*, pages 32540–32560. PMLR, 2023.
- Raphael Suter, Djordje Miladinovic, Bernhard Schölkopf, and Stefan Bauer. Robustly disentangled causal mechanisms: Validating deep representations for interventional robustness. In *International Conference on Machine Learning*, pages 6056–6065. PMLR, 2019.
- Rohan Taori, Achal Dave, Vaishaal Shankar, Nicholas Carlini, Benjamin Recht, and Ludwig Schmidt. Measuring robustness to natural distribution shifts in image classification. *Advances in Neural Information Processing Systems*, 33:18583–18599, 2020.

- Antonio Torralba and Alexei A. Efros. Unbiased look at dataset bias. In *CVPR 2011*, pages 1521–1528, Colorado Springs, CO, USA, June 2011. IEEE. ISBN 978-1-4577-0394-2. doi: 10.1109/CVPR.2011.5995347.
- Hemanth Venkateswara, Jose Eusebio, Shayok Chakraborty, and Sethuraman Panchanathan. Deep hashing network for unsupervised domain adaptation. In *Proceedings of the IEEE conference on computer vision and pattern recognition*, pages 5018–5027, 2017.
- Yoav Wald, Amir Feder, Daniel Greenfeld, and Uri Shalit. On Calibration and Out-of-Domain Generalization. In *Advances in Neural Information Processing Systems*, volume 34, pages 2215–2227. Curran Associates, Inc., 2021.
- Shen Yan, Huan Song, Nanxiang Li, Lincan Zou, and Liu Ren. Improve unsupervised domain adaptation with mixup training. *arXiv preprint arXiv:2001.00677*, 2020.
- Mengyue Yang, Zhen Fang, Yonggang Zhang, Yali Du, Furui Liu, Jean-Francois Ton, and Jun Wang. Invariant Learning via Probability of Sufficient and Necessary Causes, October 2023. arXiv:2309.12559 [cs].
- Marvin Zhang, Henrik Marklund, Nikita Dhawan, Abhishek Gupta, Sergey Levine, and Chelsea Finn. Adaptive risk minimization: Learning to adapt to domain shift. *Advances in Neural Information Processing Systems*, 34:23664–23678, 2021.
- Xin Zhang, Shixiang Shane Gu, Yutaka Matsuo, and Yusuke Iwasawa. Domain Prompt Learning for Efficiently Adapting CLIP to Unseen Domains, August 2022. arXiv:2111.12853 [cs].
- Kaiyang Zhou, Jingkang Yang, Chen Change Loy, and Ziwei Liu. Conditional Prompt Learning for Vision-Language Models, October 2022a. arXiv:2203.05557 [cs].
- Kaiyang Zhou, Jingkang Yang, Chen Change Loy, and Ziwei Liu. Learning to Prompt for Vision-Language Models. *International Journal of Computer Vision*, 130(9):2337–2348, September 2022b. ISSN 0920-5691, 1573-1405. doi: 10.1007/s11263-022-01653-1. arXiv:2109.01134 [cs].
- Roland S. Zimmermann, Yash Sharma, Steffen Schneider, Matthias Bethge, and Wieland Brendel. Contrastive Learning Inverts the Data Generating Process, April 2022. arXiv:2102.08850 [cs].

Appendix

This supplementary material provides detailed proofs for the theorem and proposition mentioned in the main text. Furthermore, additional experimental results and implementation details are provided.

- Appendix A provides the definition of all notations of the main text.
- Appendix B provides some background of the causality.
- Appendix C provides the proof of Theorem 3.1 in the main text.
- Appendix D provides the proof of Theorem 3.3 in the main text.
- Appendix E provides the proof of Proposition 4.1 in the main text.
- Appendix F provides the proof of Theorem 4.2 in the main text.
- Appendix G provides the implementation details and the pseudo-code for CLIP-ICM.
- Appendix H provides more results of CLIP-ICM in PACS and Office-Home datasets.
- Appendix I provides detailed description of the used datasets.
- Appendix J provides a detailed comparison with the existing works.
- Appendix K provides the ablation study on the hyper-parameter λ , the D_{inv} and choice of data augmentation.
- Appendix L provides an analysis where the domain prompt is used in zero-shot case.

Table 5: The definitions of all notations.

Variables	
\mathbf{x}	An image sample.
\mathbf{t}	A text description / prompt.
e	An environment.
e^*	The test environment.
c	A class.
y	A ground-truth label.
$\hat{\mathbf{z}}$	The image embedding.
$\hat{\mathbf{z}}_c$	The class-specific text embedding of class c .
\mathbf{z}	A latent factor.
\mathbf{z}_{inv}	An invariant latent factor.
\mathbf{z}_{var}	An variant latent factor.
\mathbf{w}	The normal vector of the decision boundary.
Random Variables	
X	The random variable of the image.
Y	The random variable of the class label.
Z_{inv}	The random variable of the invariant factors.
Z_{var}	The random variable of the variant factors.
Z_{var}^*	The random variable of variant factors in environment e^* .
E	The selection variable of environments.
Sample Spaces / Supports	
\mathcal{T}	The support of text description.
\mathcal{X}	The support of image samples.
$\mathcal{X}^{do(z_i)}$	The support of image samples when the latent factor z_i takes a fixed value.
\mathcal{Y}	The support of the class label.
$\hat{\mathcal{Z}}$	The support of the embedding.
\mathcal{Z}	The support of the latent factors.

A List of Notations

We list the definitions of all notations from the main text in Table 5 and Table 6.

B Background in Causality

Structural Causal Model The SCMs can be used to describe the causal variables and their relationships. The definition of SCM is:

Definition B.1. (Structural Causal Model Pearl [2009])

1. A set U of background or exogenous variables, representing factors outside the model, which nevertheless affect relationships within the model.
2. A set $V = \{V_1, \dots, V_n\}$ of endogenous variables, assumed to be observable. Each of these variables is functionally dependent on some subset PA_i of $U \cup V$. Here, PA_i means the set of parent nodes of the endogenous variable V_i .
3. A set F of functions $\{f_1, \dots, f_n\}$ such that each f_i determines the value v_i of $V_i \in V$, $v_i = f_i(pa_i, u)$. These functions are also known as **causal mechanisms**.
4. A joint probability distribution $P(u)$ over U .

The SCMs can be represented by Directed Acyclic Graphs (DAG) Glymour et al. [2016]. In the DAG, the arrow $X \rightarrow Y$ denotes that changes in the value of X directly cause changes in Y . However, this relationship does not hold in the reverse order.

The Selection Diagram and Transportability Pearl et al. Pearl and Bareinboim [2014] propose the selection diagram, which is used to model the causal relation between different environments with an external selection variable. The definition of the selection diagram is:

Table 6: The definitions of all notations.

Functions	
f_I	The image encoder.
f_T	The text encoder.
f_{I^*}	The ideal image encoder.
f_{T^*}	The ideal text encoder.
g	The ideal data-generating process.
f	The ideal representation learning process.
h	The regular predictor.
h_{inv}	The invariant predictor.
\mathbb{I}	The indicator function.
W	The coefficient matrix of a linear classifier.
\hat{Z}	The collection of embedding vectors.
P	The probability distribution.
P^*	The probability distribution in environment e^* .
$P^{do(z_i)}$	The distribution of other latent factor when $z_i \in \mathbf{z}$ takes a fixed value.
p	The probability value.
α	The data augmentation function.
Sets	
E_{tr}	The set of all training environments
E_{all}	The set of all environments
\mathcal{D}	The datasets from training environments
\mathcal{D}^e	The dataset in environments e
\mathcal{H}	The hypothesis class of regular predictor
\mathcal{H}_{inv}	The hypothesis class of the invariant predictor
Functionals	
R^{OOD}	The OOD risk.
R^e	The generalization risk in environment e .
\hat{R}^e	The empirical risk in environment e .
R_{tr}	The generalization risk on E_{tr} .
\hat{R}_{tr}	The empirical risk on E_{tr} .
R^*	The generalization risk in environment e^* .
\mathfrak{R}	The Rademacher complexity.
Constants	
D	The dimension of embedding space / latent factors.
D_{inv}	The dimension of the invariant factors.
D_{var}	The dimension of the variant factors.
N^e	The number of instances in environment e .
C	The total number of classes.
K	the Total number of data augmentations.

Definition B.2. (Selection diagram): Let $\langle M, M^* \rangle$ be a pair of SCMs relative to domain $\langle \Pi, \Pi^* \rangle$, sharing a causal diagram G . $\langle M, M^* \rangle$ is said to induce a selection diagram D if D is constructed as follows:

1. Every edge in G is also an edge in D
 2. D contains an extra edge $S_i \rightarrow V_i$ whenever there might exist a discrepancy $f_i \neq f_i^*$ or $P(U_i) \neq P^*(U_i)$ between M and M^* .
- The set S are denoted as selection variables.

Transportability aims to study whether the causal relation in a specific environment can be applied to any other environment, which is defined as:

Definition B.3. (Transportability): Let D be a selection diagram relative to domain $\langle \Pi, \Pi^* \rangle$. Let $\langle P, I \rangle$ be the pair of observational and interventional distributions of Π , and P^* be the observational

distribution of Π^* . The causal relation $R(\Pi^*) = P^*(Y|do(X))$ is said to be transportable from Π to Π^* in D if $R(\Pi^*)$ is uniquely computable from P, P^*, I in any model that induces D .

C Proof for Theorem 3.1

Before we proceed to the proof of Theorem 3.1, we first provide some useful definitions and lemma.

Definition C.1. (d -separation): A set S of nodes is said to block a path p if either

1. p contains at least one arrow-emitting node that is in S ,
2. p contains at least one collision node that is outside S and has no descendant in S .

If S blocks all paths from set X to set Y , it is said to d -separate X and Y . X and Y are independent given S , written $X \perp\!\!\!\perp Y|S$.

The d -separation reflects the conditional independencies that hold the distribution P that is compatible with the DAG.

Definition C.2. (Rules of do-calculus) Let X, Y, Z, W be arbitrary disjoint sets of nodes in a causal DAG G . We denote by $G_{\overline{X}}$ the graph obtained by deleting from G all arrows pointing to nodes in X . Likewise, we denote by $G_{\underline{X}}$ the graph obtained by deleting from G all arrows emerging from nodes in X . The notation $G_{\overline{X}\underline{Z}}$ represents the deletion of both incoming and outgoing arrows.

1. Insertion/deletion of observations.

$$P(Y|do(X), Z, W) = P(Y|do(X), W) \quad \text{if } (Y \perp\!\!\!\perp Z|X, W)_{G_{\overline{X}}}.$$

2. Action/observation exchange.

$$P(Y|do(X), do(Z), W) = P(Y|do(X), W) \quad \text{if } (Y \perp\!\!\!\perp Z|X, W)_{G_{\overline{X}\underline{Z}}}.$$

3. Insertion/deletion of actions.

$$P(Y|do(X), do(Z), W) = P(Y|do(X), W) \quad \text{if } (Y \perp\!\!\!\perp Z|X, W)_{G_{\overline{X}\underline{Z}(W)}}.$$

where $Z(W)$ is the set of Z -nodes that are not ancestors of any W -node in $G_{\overline{X}}$.

Definition C.3. (Identifiability) A causal query $Q(M) = P(Y|do(X))$ is identifiable, given a set of assumptions A , if for any two (fully specified) models, M_1 and M_2 that satisfy A , we have:

$$P(M_1) = P(M_2) \rightarrow Q(M_1) = Q(M_2)$$

Definition C.4. (Trivial transportability). A causal relation R is said to be trivially transportable from Π to Π^* , if $R(\Pi^*)$ is identifiable from (G^*, P^*) .

R is trivially transportable if we can directly estimate $R(\Pi^*)$ from observational data of Π^* , unaided by the causal information from Π . The following state the sufficient and necessary conditions of transportability of average causal effect $P^*(Y|do(X))$.

Definition C.5. (S -admissibility). A set Z of variables satisfying $(Y \perp\!\!\!\perp S|Z, X)$ in $D_{\overline{X}}$ will be called S -admissible with respect to the causal effect of X on Y . $D_{\overline{X}}$ denote deleting all arrows pointing to node X in D .

Lemma C.6. (sufficient and necessary conditions of transportability Pearl and Bareinboim [2014]) The average causal effect $P^*(Y|do(X))$ is transportable from Π to Π^* if either one of the following conditions holds:

1. $P^*(Y|do(X))$ is trivially transportable.
2. There exists a set of covariates Z (possibly affected by X) such that Z is S -admissible and for which $P^*(z|do(x))$ is transportable.
3. There exists a set of covariates, W that satisfy $(X \perp\!\!\!\perp Y|W)_{\overline{X(W)}}$ and for which $P^*(w|do(x))$ is transportable.

Proof. 1. According to Definition C.4, the causal relationship can be directly estimated from observational data of Π^* .

2. If condition 2 holds, it implies:

$$\begin{aligned} P^*(Y|do(X)) &= P(Y|do(X), S) \\ &= \sum_Z P(Y|do(X), Z, S)P(Z|do(X), S) \\ &= \sum_Z P(Y|do(X), Z)P^*(Z|do(X)) \end{aligned} \tag{13}$$

The transportability of $P(Z|do(X))$ reduces $P^*(Z|do(X))$ to a star-free expression and therefore $P^*(Y|do(X))$ is transportable. 3. If condition 3 holds, it implies:

$$\begin{aligned} P^*(Y|do(X)) &= P(Y|do(X), S) \\ &= \sum_W P(Y|do(X), W, S)P(W|do(X), S) \\ &= \sum_W P(Y|W, S)P^*(W|do(X)) \end{aligned} \quad (14)$$

According to Rule 3 of Definition C.2, the transportability of $P^*(W|do(X))$ would render $P(W|do(X), S)$ to a star-free expression and render $P^*(Y|do(X))$ transportable. This ends the proof. \square

We are now prepared to present the proof for Theorem 3.1 in the main text:

Theorem C.7. *Let the distribution $P^*(\cdot) := P(\cdot|E = e^*)$ be the distribution on the test environment $E = e^*$. The causal mechanism $P^*(Y|X)$ can be computed with:*

$$P^*(Y|X) = \sum_{Z_{var}} \sum_{Z_{inv}} P(Y|Z_{var}, Z_{inv})P(Z_{inv}|X)P^*(Z_{var}|X). \quad (15)$$

Proof. The causal mechanism we would like to estimate is:

$$\begin{aligned} P^*(Y|do(X)) &= P(Y|do(X), E = e^*) \\ &= \sum_{Z_{inv}} \sum_{Z_{var}} P(Y|do(X), Z_{var}, Z_{inv}, E = e^*) \\ &\quad P(Z_{var}|do(X), E = e^*)P(Z_{inv}|do(X), E = e^*) \end{aligned} \quad (16)$$

From the Rule 1 of Definition C.2, we have

$$P(Y|do(X), Z_{var}, Z_{inv}, E = e^*) = P(Y|do(X), Z_{var}, Z_{inv}), \quad (17)$$

because Z_{var} satisfies $(Y \perp\!\!\!\perp E|Z_{var}, X)$ in $D_{\overline{X}}$, and according to Definition C.5, the Z_{var} E -admissible with respect to the causal effect of X on Y . Then, since $(Y \perp\!\!\!\perp X|Z_{var}, Z_{inv})$, the following holds:

$$P(Y|do(X), Z_{var}, Z_{inv}) = P(Y|Z_{var}, Z_{inv}) \quad (18)$$

According to Definition C.1, $Z_{inv} \rightarrow Y \leftarrow Z_{var} \leftarrow E$ is a collision node:

$$P(Z_{inv}|do(X), E = e^*) = P(Z_{inv}|do(X)). \quad (19)$$

And since there is no other path from $X \rightarrow Z_{inv}$ and $X \rightarrow Z_{var}$, the do -operator is trivial. Therefore, the Equation (16) can be rewrite as:

$$P^*(Y|do(X)) = \sum_{Z_{inv}} \sum_{Z_{var}} P(Y|Z_{var}, Z_{inv})P(Z_{inv}|X)P^*(Z_{var}|X) \quad (20)$$

This ends the proof. \square

D Proof for Theorem 3.3

Before we proceed to the proof of Theorem 3.3, we give a definition to the Rademacher Complexity.

Definition D.1. (Rademacher Complexity Mohri et al. [2018]) Let \mathcal{H} be a family of functions from \mathcal{Z} to $[0, 1]$ and $S = (z_1, \dots, z_m)$ a fixed sample of size m with elements in \mathcal{Z} . Let \mathcal{D} denote the distribution according to which samples are drawn. For any integer $m \geq 1$, the Rademacher complexity of a hypothesis class \mathcal{H} is the expectation of the empirical Rademacher complexity over all samples of size m drawn from \mathcal{D} :

$$\begin{aligned} \mathfrak{R}(\mathcal{H}) &= \mathbb{E}_{S \sim \mathcal{D}^m} [\hat{\mathfrak{R}}(\mathcal{H})], \text{ where} \\ \hat{\mathfrak{R}}(\mathcal{H}) &= \mathbb{E}_{\sigma} \left[\frac{1}{m} \sup_{h \in \mathcal{H}} \sum_{i=1}^m \sigma_i h(z_i) \right], \end{aligned} \quad (21)$$

where σ_i s are independent uniform random variables taking values in $\{-1, +1\}$ and x_1, \dots, x_m are the components of vector \mathbf{x} .

Next, we are going to show how the generalization risk in E_{tr} can be related to a test environment $e^* \in E_{all}$ with the $\mathcal{H}\Delta\mathcal{H}$ -divergence.

Lemma D.2. (Ben-David et al., 2010 Ben-David et al. [2010]) For all hypothesis $h \in \mathcal{H}$, the risk on P^* is bounded as:

$$R^*(h) \leq R_{tr}(h) + d_{\mathcal{H}\Delta\mathcal{H}}(P, P^*) + \lambda_{\mathcal{H}}, \quad (22)$$

where $\lambda_{\mathcal{H}}$ is the best joint risk:

$$\lambda_{\mathcal{H}} := \inf_{h' \in \mathcal{H}} [R_{tr}(h') + R^*(h')]/2. \quad (23)$$

Proof. By the definition of $d_{\mathcal{H}\Delta\mathcal{H}}(P, P^*)$,

$$d_{\mathcal{H}\Delta\mathcal{H}}(P, P^*) = \sup_{h, h' \in \mathcal{H}} |R_{tr}(h, h') - R^*(h, h')| \geq |R_{tr}(h, h') - R^*(h, h')| \quad (24)$$

Also, with the triangle inequality for classification error:

$$\begin{aligned} R^*(h) &\leq R^*(h') + R^*(h, h') \\ &\leq R^*(h') + R_{tr}(h, h') + |R_{tr}(h, h') - R^*(h, h')| \\ &\leq R^*(h') + R_{tr}(h, h') + d_{\mathcal{H}\Delta\mathcal{H}}(P, P^*) \\ &\leq R^*(h') + R_{tr}(h) + R_{tr}(h') + d_{\mathcal{H}\Delta\mathcal{H}}(P, P^*) \\ &\leq R_{tr}(h) + d_{\mathcal{H}\Delta\mathcal{H}}(P, P^*) + \lambda_{\mathcal{H}}. \end{aligned} \quad (25)$$

This ends the proof. \square

Now we can proof Theorem 3.3 from the main text.

Theorem D.3. Let the empirical risk gap $\hat{R}_{tr}(h) - \hat{R}_{tr}(h_{inv}) = \mathcal{C}_1$, and the Rademacher complexity gap $\mathfrak{R}(\mathcal{H}) - \mathfrak{R}(\mathcal{H}_{inv}) = \mathcal{C}_2$. If $d_{\mathcal{H}\Delta\mathcal{H}}(P, P^*) > \mathcal{C}_1 - \mathcal{C}_2$, $\forall e^* \in E_{all}, e^* \notin E_{tr}$. Then, the OOD risk of the invariant predictor is lower than that of the regular predictor:

$$R^{\text{OOD}}(h_{inv}) < R^{\text{OOD}}(h), \quad \forall h_{inv} \in \mathcal{H}_{inv}, h \in \mathcal{H}. \quad (26)$$

Proof. According to Lemma D.2, $\forall e^* \in E_{all}, e^* \notin E_{tr}$, the following holds for all $h \in \mathcal{H}$:

$$R^*(h) \leq R_{tr}(h) + d_{\mathcal{H}\Delta\mathcal{H}}(P, P^*) + \lambda_{\mathcal{H}}, \quad (27)$$

According to Equation (1) and Equation (9), the OOD risk of \mathcal{H} is:

$$\begin{aligned} R^{\text{OOD}}(h) &= \max_{e^* \in E_{all}} R^*(h) \\ &= \max_{e^* \in E_{all}, e^* \notin E_{tr}} R^*(h) \\ &\leq \max_{e^* \in E_{all}, e^* \notin E_{tr}} R_{tr}(h) + d_{\mathcal{H}\Delta\mathcal{H}}(P, P^*) + \lambda_{\mathcal{H}} \\ &\leq \max_{e^* \in E_{all}, e^* \notin E_{tr}} \hat{R}_{tr}(h) + d_{\mathcal{H}\Delta\mathcal{H}}(P, P^*) + \lambda_{\mathcal{H}} + \mathfrak{R}(\mathcal{H}) + \sqrt{\frac{\log \frac{1}{\delta}}{N}}. \end{aligned} \quad (28)$$

Since the distribution $P^*(Z_{inv})$ and $P(Z_{inv})$ are the same. $\forall e^* \in E_{all}, e^* \notin E_{tr}$ the following holds for all $h_{inv} \in \mathcal{H}_{inv}$:

$$R^*(h_{inv}) = R_{tr}(h_{inv}). \quad (29)$$

And the OOD risk of $h_{inv} \in \mathcal{H}_{inv}$ is:

$$\begin{aligned} R^{\text{OOD}}(h_{inv}) &= R_{tr}(h_{inv}) \\ &\leq \hat{R}_{tr}(h_{inv}) + \mathfrak{R}(\mathcal{H}_{inv}) + \sqrt{\frac{\log \frac{1}{\delta}}{N}}. \end{aligned} \quad (30)$$

Minus Equation (30) from Equation (28) from both sides, the term $\sqrt{\frac{\log \frac{1}{\delta}}{N}}$ cancel out, and the gap between $R^{\text{OOD}}(h_{inv})$ and $R^{\text{OOD}}(h)$ depends on \mathcal{C}_1 and \mathcal{C}_2 . This ends the proof. \square

E Proof for Proposition 4.1

Building upon prior works Roeder et al. [2021], Ahuja et al. [2022b], Hyvarinen and Morioka [2016], Zimmermann et al. [2022], we offer proof demonstrating that CLIP identifies latent factors up to an invertible linear transformation, and we also reuse some of their proof techniques.

Proposition E.1. *Consider the data generating process of CLIP as an injective function, where $\mathbf{x} = g(\mathbf{z})$, $\mathbf{z} \sim P(Z)$. Suppose there exists an ideal encoder $f_{I^*} : \mathcal{X} \rightarrow \mathcal{Z}$, such that $f_{I^*}(\mathbf{x}) = g^{-1}(\mathbf{x}) = \mathbf{z}$. Here I^* is the ideal parameter of the image encoder; T^* is the ideal parameter of the text encoder. Let $\mathcal{Z} \subset \mathbb{R}^D$, if $|\mathcal{T}| \geq (1 + \sqrt{1 + 8D})/2$ in E_{tr} , and the loss function is minimized, where the prediction results of the learned encoder f_I is the same as the ideal encoder f_{I^*} . Then the learned encoder $f_I(\mathbf{x})$ identifies the latent factor \mathcal{Z} up to an invertible linear transformation A , i.e. $f_I(\mathbf{x}) = A\mathbf{z}$.*

Proof. We proceed by revisiting the pre-training process of CLIP. CLIP aims to train an image encoder f_I and a text encoder f_T to map \mathbf{x} and \mathbf{t} into a joint embedding space $f_I(\mathbf{x}), f_T(\mathbf{t}) \in \mathbb{R}^d$. Given a mini-batch of N image-text pairs $\{\mathbf{x}_i, \mathbf{t}_i\}_{i=1}^N$, the objective for learning f_I and f_T is achieved by the following contrastive loss functions:

$$\begin{aligned}\mathcal{L}_I &= -\frac{1}{N} \log \sum_{i=1}^N \frac{\exp(f_I(\mathbf{x}_i)^T f_T(\mathbf{t}_i)/\tau)}{\sum_{j=1}^N \exp(f_I(\mathbf{x}_i)^T f_T(\mathbf{t}_j)/\tau)}, \\ \mathcal{L}_T &= -\frac{1}{N} \log \sum_{i=1}^N \frac{\exp(f_T(\mathbf{t}_i)^T f_I(\mathbf{x}_i)/\tau)}{\sum_{j=1}^N \exp(f_T(\mathbf{t}_i)^T f_I(\mathbf{x}_j)/\tau)},\end{aligned}\tag{31}$$

where τ is a temperature hyper-parameter.

Minimizing the loss function in Equation (31) means that for a fixed text encoder f_T , for any pair of $(\mathbf{x}_i, \mathbf{t}_i)$ in the training set, the following holds:

$$\frac{\exp(f_I(\mathbf{x}_i)^T f_T(\mathbf{t}_i)/\tau)}{\sum_{j=1}^N \exp(f_I(\mathbf{x}_i)^T f_T(\mathbf{t}_j)/\tau)} = \frac{\exp(f_{I^*}(\mathbf{x}_i)^T f_{T^*}(\mathbf{t}_i)/\tau)}{\sum_{j=1}^N \exp(f_{I^*}(\mathbf{x}_i)^T f_{T^*}(\mathbf{t}_j)/\tau)},\tag{32}$$

which means that we can construct a tuple $(\mathbf{t}_a, \mathbf{t}_b)$ form of distinct text description \mathbf{t} . This means we can divide the above equation and cancel out the normalizing term and get:

$$\frac{\exp(f_I(\mathbf{x})^T f_T(\mathbf{t}_a))}{\exp(f_I(\mathbf{x})^T f_T(\mathbf{t}_b))} = \frac{\exp(f_{I^*}(\mathbf{x})^T f_{T^*}(\mathbf{t}_a))}{\exp(f_{I^*}(\mathbf{x})^T f_{T^*}(\mathbf{t}_b))}.\tag{33}$$

Taking the logarithm of both sides, this simplifies to:

$$(f_T(\mathbf{t}_a) - f_T(\mathbf{t}_b))^T f_I(\mathbf{x}) = (f_{T^*}(\mathbf{t}_a) - f_{T^*}(\mathbf{t}_b))^T f_{I^*}(\mathbf{x}).\tag{34}$$

By repeating Equation (34) D times and by the diversity condition noted above, the resulting difference vectors are linearly independent. Repeating Equation (34) D times require there exists at least D combinations of tuple $(\mathbf{t}_a, \mathbf{t}_b)$ in the training set, which means that $\frac{N(N-1)}{2} \geq D$. Solve this for the value of N , we obtain that $N \geq (1 + \sqrt{1 + 8D})/2$. We collect these vectors together as the columns of $D \times D$ -dimensional matrices L and L' , forming the following system of d linear equations:

$$f_I(\mathbf{x}) = (L'L^{-1})^T f_{I^*}(\mathbf{x}).\tag{35}$$

Therefore, $f_I(\mathbf{x}) = Af_{I^*}(\mathbf{x}) = A\mathbf{z}$ where $A = L'L^{-1}$ is invertible. This ends the proof. \square

F Proof for Theorem 4.2

Theorem F.1. *Consider observational data generated from an injective mapping $g : \mathcal{Z} \rightarrow \mathcal{X}$, where the latent factors Z follow a distribution $P(Z)$ supported on \mathcal{Z} . If a do-intervention is applied to the i -th latent factor z_i to take a fixed value, with the distribution of other latent factors denoted as $P^{\text{do}(z_i)}(Z)$, the resulting distribution of the interventional data is denoted as $P^{\text{do}(z_i)}(X)$. Suppose that an encoder f_I satisfies Proposition 4.1, and the output of the k^{th} component of the encoder is required to take a fixed value $f_I(\mathbf{x})[k] = z_i^{\dagger}$ for all $\mathbf{x} \in \mathcal{X}^{\text{do}(z_i)}$. Then, the encoder identifies the intervened latent z_i up to a shift and scaling, i.e., $f_I(\mathbf{x})[k] = a_i z_i + b_i$, where $a_i \in \mathbb{R}$ and $b_i \in \mathbb{R}$.*

Proof. The encoder f_I satisfies Proposition 4.1 implies that $f_I(\mathbf{x}) = AZ$. The k -th element of $f_I(\mathbf{x})[k] = A_{k,:}Z, \forall z \in \mathcal{Z}$. Considering the support of the distribution of the unintervened latent $P^{do(z_i)}(Z)$ is a non-empty subset. We separately write the intervened latent as $Z = [z_i, Z_{i:}]$, where z_i is the intervened latent and $Z_{i:}$ is the set of other latent factors other than z_i . Then, $f_I(\mathbf{x})[k]$ can be written as:

$$f_I(\mathbf{x})[k] = A_{k,i} \cdot z_i + A_{k,i:}Z_{i:} + b_i, \quad (36)$$

where $A_{k,i}$ represents the i -th element of the k -th row, and $A_{k,i:}$ denotes the k -th row excluding the i -th element. If the output of the k -th component of the encoder to have a fixed value of z^\dagger , then setting $f_I(\mathbf{x})[k] = z^\dagger$ yields the following:

$$z^\dagger = A_{k,i} \cdot z_i + A_{k,i:}Z_{i:} + b_i. \quad (37)$$

Consider another data point Z' from the interventional distribution $P^{do(z_i)}Z$. We can express Z' as $Z' = [z_i, Z'_{i:}]$. The Z' is nearly identical to Z , except for $Z'_{i:}$, which is obtained by adding $\delta \mathbf{e}_j$ to $Z_{i:}$. Here, δ is a small positive value, and \mathbf{e}_j represents a one-hot vector with the j -th element as one and the others as zero.

$$z^\dagger = A_{k,i} \cdot z_i + A_{k,i:}Z'_{i:}. \quad (38)$$

If we use Equation (37) minus Equation (38), the results are as followed:

$$\begin{aligned} A_{k,i:}Z'_{i:} &= A_{k,i:}Z_{i:} \\ A_{k,i:}(Z'_{i:} - Z_{i:}) &= 0 \\ \delta A_{k,i:}\mathbf{e}_j &= 0. \end{aligned} \quad (39)$$

This implies the j -th element in $A_{k,i:}$ is zero. Iterative apply j to the $Z_{i:}$ can proof that $A_{k,i:}$ is zero, which makes $f_I(\mathbf{x})[k] = A_{k,i}z_i$. This ends the proof. \square

G Implementation of CLIP-ICM

G.1 Implementation Details.

We utilize two types of evaluation protocols introduced in Equation (2) and Equation (3). In linear-probe prediction, we follow the leave-one-out evaluation protocol, where one domain is chosen as the test domain and the other domains are chosen as the training domains. While in zero-shot prediction, despite CLIP-ICM not requiring labeled data, we also follow this leave-one-out protocol to avoid information from the test domain. We employ 7 data augmentation techniques, i.e. ColorJitter, GrayScale, GaussianBlur, RandomInvert, RandomPosterize, RandomSolarize, and RandomEqualize for producing interventional data. The matrix C_ξ is obtained by solving a low-rank approximation problem through singular value decomposition. For the linear-probe evaluation, the classifier undergoes training for a maximum of 1000 epochs with an l_1 penalty of $1e^{-4}$ implementing with the built-in function of Scikit-learn Kramer [2016]. It is noteworthy that we learn C_ξ in a totally unsupervised manner without the inclusion of label information. Additionally, during the estimating of C_ξ , there are no images from the target domain included. The detailed algorithm is illustrated in Appendix G.2 and the conducting code is provided in the supplementary materials. All experiments are conducted on a single NVIDIA-RTX A6000 GPU, and the average training duration for each result is less than one hour.

G.2 Pseudo Code

The pseudo code of CLIP-ICM is illustrated in Algorithm 1.

H More Results on Domainbed

In this section, we provide more results on datasets from the Domainbed benchmark in Table 7 and Table 3. From the tables, we observe that the results of zero-shot and linear-probe of CLIP-ICM consistently improve the performance of the original CLIP model in both the PACS and Office-Home datasets.

Algorithm 1 CLIP-ICM

Require: CLIP image encoder f_I and images from training domain $\mathbf{x} \in \mathcal{D}$, $\mathcal{D} = \{\mathcal{D}^e\}_{e \in E_{tr}}$. K types of data augmentation $\mathcal{A} = \{\alpha_k\}_{k=1}^K$. Hyperparameter λ and D_{inv} .

- 1: Initialize the container $\hat{Z} = []$ for original representation
 - 2: Initialize the container $\hat{Z}' = []$ for intervened representation
 - 3: **for** \mathbf{x} in \mathcal{D} **do**
 - 4: Sample random augmentation α_k from K
 - 5: Get the original image representation $\hat{z} = f_I(\mathbf{x})$
 - 6: Get $\mathbf{x}^{do(k)} = \alpha_k(\mathbf{x})$
 - 7: Get the intervened representation $\hat{z}' = f_I(\mathbf{x}^{do(k)})$
 - 8: Append \hat{z} into \hat{Z}
 - 9: Append \hat{z}' into \hat{Z}'
 - 10: **end for**
 - 11: Get the correlation matrix $Corr = \hat{Z}^T \hat{Z} - \lambda \cdot (\hat{Z} - \hat{Z}')^T (\hat{Z} - \hat{Z}')$. $\hat{Z} \in \mathbb{R}^{N \times d}$, $\hat{Z}' \in \mathbb{R}^{N \times d}$, $Corr \in \mathbb{R}^{d \times d}$
 - 12: Perform Singular Value Decomposition (SVD) for $Corr$ to get U, V, Σ
 - 13: Get the highest D_{inv} singular vector $U_{:D_{inv},:} \in \mathbb{R}^{D_{inv} \times D}$
- Output:** The target transform C_ξ is $U_{:D_{inv},:}$.

Table 7: Accuracy on PACS dataset. **A,C,P** and **S** represents different domains.

Algorithm	Backbone	P	A	C	S	Avg
ERM	R50	97.2±0.3	84.7±0.4	80.8±0.6	79.3±1.0	85.5
IRM Arjovsky et al. [2020]	R50	96.7±0.6	84.8±1.3	76.4±1.1	76.1±1.0	83.5
GroupDRO Sagawa* et al. [2019]	R50	96.7±0.3	83.5±0.9	79.1±0.6	78.3±2.0	84.4
Mixup Yan et al. [2020]	R50	97.6±0.1	86.1±0.5	78.9±0.8	75.8±1.8	84.6
MMD Li et al. [2018]	R50	96.6±0.2	86.1±1.4	79.4±0.9	76.5±0.5	84.6
DANN Ganin et al. [2016]	R50	97.3±0.4	86.4±0.8	77.4±0.8	73.5±2.3	83.6
ARM Zhang et al. [2021]	R50	97.4±0.3	86.8±0.6	76.8±0.5	79.3±1.2	85.1
MBDG Robey et al. [2021]	R50	97.0	80.6	79.3	85.2	85.6
CLIP Linear-probe	R50	99.2±0.7	91.7±0.8	92.5±0.7	82.3±0.2	91.4
CLIP-ICM Linear-probe	R50	99.4±0.5	92.8±0.7	93.9±0.4	83.8±0.5	92.5
CLIP Linear-probe	ViT-B	97.3±0.7	98.4±0.1	99.5±0.4	90.4±0.3	96.4
CLIP-ICM Linear-probe	ViT-B	98.8±0.2	99.4±0.3	99.8±0.8	92.1±0.5	97.5
CLIP Zero-shot	R50	99.3±0.0	91.0±0.0	93.1±0.0	80.5±0.0	91.0
CLIP-ICM Zero-shot	R50	99.4±0.4	93.6±0.2	99.3±0.5	83.1±0.6	93.8
CLIP Zero-shot	ViT-B	100.0±0.0	97.4±0.0	99.2±0.0	88.1±0.0	96.1
CLIP-ICM Zero-shot	ViT-B	98.7±0.5	99.1±0.4	99.9±0.1	91.7±0.4	97.3

I Dataset Details

DOMAINBED includes downloaders and loaders for seven multi-domain image classification tasks:

- **PACS** Li et al. [2017] comprises four domains $e \in \{\text{art, cartoons, photos, sketches}\}$. This dataset contains 9,991 examples of dimension (3, 224, 224) and 7 classes.
- **VLCS** Fang et al. [2013] comprises photographic domains $e \in \{\text{Caltech101, LabelMe, SUN09, VOC2007}\}$. This dataset contains 10,729 examples of dimension (3, 224, 224) and 5 classes.
- **Office-Home** Venkateswara et al. [2017] includes domains $e \in \{\text{art, clipart, product, real}\}$. This dataset contains 15,588 examples of dimension (3, 224, 224) and 65 classes.
- **Terra Incognita** Beery et al. [2018] contains photographs of wild animals taken by camera traps at locations $e \in \{\text{L100, L38, L43, L46}\}$. Our version of this dataset contains 24,788 examples of dimension (3, 224, 224) and 10 classes.

Table 8: Accuracy on Office-Home dataset. **A,C,P** and **R** represents different domains.

Algorithm	Backbone	A	C	P	R	Avg
ERM	R50	61.3±0.7	52.4±0.3	75.8±0.1	76.6±0.3	66.5
IRM Arjovsky et al. [2020]	R50	58.9±2.3	52.2±1.6	72.1±2.9	74.0±2.5	64.3
GroupDRO Sagawa* et al. [2019]	R50	60.4±0.7	52.7±1.0	75.0±0.7	76.0±0.7	66.0
Mixup Yan et al. [2020]	R50	62.4±0.8	54.8±0.6	76.9±0.3	78.3±0.2	68.1
MMD Li et al. [2018]	R50	60.4±0.2	53.3±0.3	74.3±0.1	77.4±0.6	66.3
DANN Ganin et al. [2016]	R50	59.9±1.3	53.0±0.3	73.6±0.7	76.9±0.5	65.9
ARM Zhang et al. [2021]	R50	58.9±0.8	51.0±0.5	74.1±0.1	75.2±0.3	64.8
SIG Li et al. [2024]	R50	76.4	63.9	85.4	85.8	77.8
CLIP Linear-probe	R50	68.0±0.8	46.3±0.3	80.4±0.9	81.9±0.7	69.1
CLIP-ICM Linear-probe	R50	78.3±0.3	56.4±0.8	88.6±0.8	87.7±0.7	77.8
CLIP Linear-probe	ViT-B	78.9±0.9	69.3±0.9	90.3±0.3	89.0±0.2	81.9
CLIP-ICM Linear-probe	ViT-B	84.3±0.5	71.4±0.2	92.5±0.2	90.2±0.8	84.6
CLIP Zero-shot	R50	71.3±0.0	50.4±0.0	81.7±0.0	82.6±0.0	71.5
CLIP-ICM Zero-shot	R50	72.6±0.4	55.0±0.9	83.2±0.3	83.7±0.8	73.6
CLIP Zero-shot	ViT-B	83.3±0.0	65.3±0.0	89.0±0.0	89.3±0.0	81.7
CLIP-ICM Zero-shot	ViT-B	83.7±0.7	67.4±0.6	90.8±0.9	90.1±0.6	82.6

- **DomainNet** Peng et al. [2019] has six domains $e \in \{\text{clipart, infograph, painting, quickdraw, real, sketch}\}$. This dataset contains 586,575 examples of size (3, 224, 224) and 345 classes.

For all datasets, we first pool the raw training, validation, and testing images together. For each random seed, we then instantiate random training, validation, and testing splits.

J More comparison with related works

J.1 Invariant Risk Minimization Arjovsky et al. [2020]

Invariant Risk Minimization (IRM) and IRM-based methods Ahuja et al. [2022a], Yang et al. [2023] also aim to minimize the OOD risks with an invariant predictor. However, note that these methods obtain invariant predictors without identifying the invariant factors. Moreover, as suggested in Figure 2 of Arjovsky et al. 2020 Arjovsky et al. [2020], there are multiple solutions to the IRM objective. Therefore finding an IRM solution doesn't mean the identification of Z_{inv} . Compared to these methods, our method ensures the identification of Z_{inv} and can perform invariant prediction in a zero-shot manner.

J.2 Model-based Domain Generalization Robey et al. [2021]

Model-based Domain Generalization Robey et al. [2021] also also proposes an SCM, their analysis method is different from ours. They believe that in domain shift, an instance X^e is generated by an underlying random variable X and e jointly passing through a domain-transfer model $G(X, e)$. In our causal diagram analysis, we believe that the sample is generated by Z_{var} and Z_{inv} jointly.

MBDG obtains the invariant features by utilizing a pre-trained domain-transfer model to constrain the distance between the features extracted by the feature extractor and the representations generated by the domain-transfer model.

In contrast, our approach learns a linear transformation of the pre-trained representation to obtain features that are invariant to data augmentation. We provide the comparison results between our method and MBDG in Table 2 and Table 7.

J.3 On Calibration and Out-of-domain Generalization Wald et al. [2021]

From the perspective of SCM analysis, Wald et al. [2021] proposes a causal graph that categorizes features into X_{causal} , $X_{ac-spurious}$, and $X_{ac-non-spurious}$. This categorization is based on the understanding that certain variables have a direct causal influence on the outcome Y . In contrast, our proposed causal graph incorporates the environmental variable E as an indirect causal pathway to Y .

From the methodological standpoint, the article addresses the OOD problem by proposing the need to find a classifier f such that $Y \perp E|f(X)$, which implies that the classifier f is calibrated. Similar to IRM, the article introduces a loss function called CLOvE designed to constrain classifiers across different domains to produce consistent results. Our approach, however, does not require modifications to the backbone model, nor do we necessitate the training of additional classifiers. Instead, we achieve a zero-shot classifier that remains invariant across each domain.

J.4 Subspace Identification Guarantee Li et al. [2024]

From the perspective of SCM analysis, SIG views the data generation process through 4 kinds of latent factors. In our SCM, Z_{inv} can be regarded as a domain-invariant variable, and Z_{var} can be regarded as a domain-variant variable. Since in our causal diagram, Y represents the description of the picture, therefore, we do not distinguish between label-irrelevant and label-relevant variables in our modeling.

From a methodological perspective, SIG uses an end-to-end, reconstruction-based network, while we use a pre-trained CLIP backbone network. SIG uses a variation-inference method to identify latent factors, while we use an intervention method to identify latent factors.

We present the performance of our method alongside the SIG’s approach to the Office-Home dataset in Table 8. Both our method and the SIG’s method utilize the ResNet50 architecture as the backbone network. Similarly, the performance on the DomainNet dataset is compared in Table 9, with both our method and the SIG’s method employing the ResNet101 backbone network.

Table 9: Comparison results on DomainNet dataset with ResNet101 backbone.

Algorithm	Backbone	Clipart	Infograph	Painting	Quickdraw	Real	Sketch	Avg
SIG Li et al. [2024]	R101	72.7	32.0	61.5	20.5	72.4	59.5	53.0
CLIP-ICM Linear-probe	R101	73.6	38.2	69.4	19.2	74.1	65.5	56.6

J.5 Domain Prompt Learning Zhang et al. [2022]

Zhang et al. [2022] introduces Domain Prompt Learning (DPL), a novel approach that improves the domain generalization performance of the CLIP model on various datasets by generating conditional prompts, achieving higher accuracy without fine-tuning the entire model. Compared with our method, also includes training a fully connected network with label information in the objective function. We provide the comparison results below:

Table 10: Comparison between our method and DPL across various datasets.

Method	VLCS	PACS	OfficeHome	Terra	Avg
CLIP Linear-Probe	78.7	96.4	81.9	60.2	79.3
CLIP + DPL Zhang et al. [2022]	84.3	97.3	84.2	52.6	79.6
CLIP-ICM Linear-Probe	86.5	97.5	84.6	64.3	83.2

J.6 Self-Supervised Learning with Data Augmentations Provably Isolates Content from Style Kugelgen et al. [2021]

Kugelgen et al. [2021] also interpret data augmentations as counterfactuals, and use them to obtain the invariant factors. Our work differs from theirs in three key aspects: the background setting, the research problem, and the implementation method.

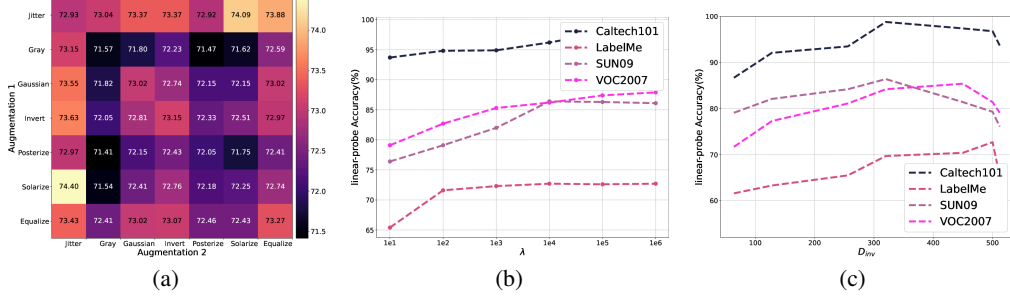


Figure 5: The experimental results for ablation studies. (a) The zero-shot accuracy of CLIP-ICM on the LabelMe domain of the VLCS dataset with different combinations of augmentations, and brighter colors indicate a higher accuracy. (b) The linear-probe accuracies of CLIP-ICM on the VLCS dataset with different λ . (c) The accuracy of CLIP-ICM on VLCS with different choice of D_{inv}

Firstly, the problem studied by Kügelgen et al. [2021] is set within the framework of self-supervised contrastive learning. In their paper, the term "invariant factor" refers to the invariant parts derived from two different augmented perspectives within a positive sample pair. In contrast, the "invariant factor" in our paper refers to the latent factors that remain unchanged across different domains. Due to the diversity of augmentation methods employed in self-supervision Chen et al. [2020], the invariant factors they investigate do not align with the invariant factors we examine.

Secondly, in their paper, they consider an in-distribution problem, where all representations Z belong to the same distribution $Z \sim P(Z)$, and they do not take into account the different distributions across various domains. In our paper, however, we investigate an out-of-distribution problem. We posit that the distribution of Z_{var} is influenced by the environment, meaning that $P(Z_{var}) \neq P^*(Z_{var})$.

Lastly, their experiments are solely based on analyzing the capabilities of SimCLR to identify latent factors, without proposing any new methods. In contrast, based on our theoretical analysis, we proposed a novel method for identifying invariant representations.

K Ablation Study

K.1 The impact of different data augmentation

We investigate how CLIP-ICM performs with varying data augmentation strategies on the VLCS dataset. The experiments include different combinations of augmentation techniques and the zero-shot prediction accuracy on the LabelMe domain is illustrated in Figure 5(a). The diagonal of Figure 5(a) indicates scenarios where only one augmentation is applied, while other cells represent combinations of data augmentation techniques. It is noteworthy that the use of data augmentation significantly improves zero-shot performance, with certain combinations showing even more promising results.

K.2 The impact of hyperparameter λ .

We conduct experiments on the VLCS dataset and visualize the results in Figure 5(b). From the results, we can observe that λ has a significant impact on the prediction results. This is because that higher value of λ indicates the second term of Equation (12) is more important and has a higher impact. These results illustrating the effectiveness of our proposed method.

K.3 Ablation study on dimension of Z_{inv}

As we mentioned at Section 4, the dimension D_{inv} of Z_{inv} is a hyperparameter. To investigate the influence of D_{inv} , we conduct an ablation study regarding the choice of D_{inv} . All results are the zero-shot performance of CLIP-ICM, conducted on the VLCS dataset with ViT-B/16 as the backbone, where $D_{inv} < 512$. The results are shown in Figure 5(c).

From Figure 5(c) we can see that as the D_{inv} increases, the accuracy first increases, and stabilizes, and slowly decreases, and finally drops. Therefore, the optimum dimension of D_{inv} should be around 300 to 350 for all domains in VLCS.

L An analysis of the zero-shot prediction with domain prompt

Table 11: Comparison results of zero-shot performance of CLIP with domain prompt in PACS dataset. \uparrow denotes that the results of CLIP with domain prompt are higher than standard prompt, while \downarrow denotes that the results of CLIP with domain prompt are lower than standard prompt.

Algorithm	Photo	Art	Cartoon	Sketch	Avg
CLIP	100.0	97.4	99.2	88.1	96.1
CLIP + Domain Prompt	100.0 –	97.4 –	99.0 \downarrow	90.2 \uparrow	96.6 \uparrow
CLIP-ICM	98.7	99.1	99.9	91.7	97.3

Table 12: Comparison results of zero-shot performance of CLIP with domain prompt in VLCS dataset. \uparrow denotes that the results of CLIP with domain prompt are higher than standard prompt, while \downarrow denotes that the results of CLIP with domain prompt are lower than standard prompt.

Algorithm	Caltech101	LabelMe	SUN09	VOC2007	Avg
CLIP	99.9	70.1	73.5	86.1	82.4
CLIP + Domain Prompt	99.2 \downarrow	69.7 \downarrow	65.1 \downarrow	80.3 \downarrow	78.5 \downarrow
CLIP-ICM	100.0	74.7	74.5	87.1	84.1

Table 13: Comparison results of zero-shot performance of CLIP with domain prompt in Office-Home dataset. \uparrow denotes that the results of CLIP with domain prompt are higher than standard prompt, while \downarrow denotes that the results of CLIP with domain prompt are lower than standard prompt.

Algorithm	Art	Clipart	Product	Real	Avg
CLIP	83.3	65.3	89.0	89.3	81.7
CLIP + Domain Prompt	82.4 \downarrow	67.0 \uparrow	87.8 \downarrow	88.7 \downarrow	81.4 \downarrow
CLIP-ICM	83.7	67.4	90.8	90.1	82.6

According to the causal analysis in Section 3.3 and the Theorem 3.1, the embedding of the text description in the test domain can be considered as the w_y^* in Equation (5).

In experiments from Section 5, we use the standard text prompt template when performing zero-shot prediction, i.e. "A photo of [cls]" where [cls] is the name of the corresponding class.

To explore the influence of text prompts on zero-shot prediction, we conducted experiments using the PACS, VLCS, and Office-Home datasets. In these experiments, we employed text prompts that incorporate domain information. For datasets where the domain names hold particular significance, such as PACS and Office-Home, we utilized the prompt 'A [domain] of [cls]'. In contrast, for the VLCS dataset, where the domain names do not have specific meanings, we adopted the prompt 'A photo of [cls] in [domain]'. Here, [domain] represents the name of the test domain. The results are illustrated in Table 11, Table 12 and Table 13.

It is important that the objective of domain generalization is to evaluate the performance of a model on unseen domains. Therefore, incorporating domain information, such as (a sketch of [cls]) would not align with the requirements of the domain generalization task. And we only conduct this experiment for exploration.

From the results in Table 11, we find that only in some domains, incorporating domain information in the prompt template can improve the zero-shot performance, such as Sketch in PACS, and Clipart in Office-Home. However, in most domains, where the domain name doesn't provide any information, or can't describe the domain properly, the performance is lower than the original template.

Another important observation is that CLIP-ICM consistently improves the performance of CLIP in most domains, without any domain related information or other kinds of template design.